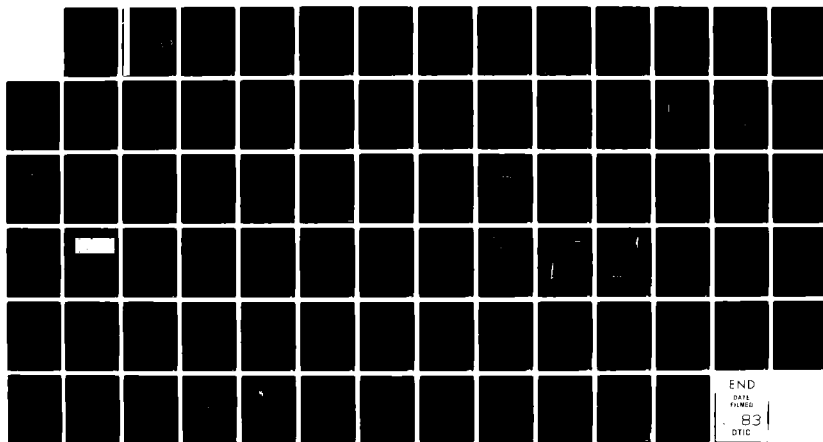


AD-A123 887

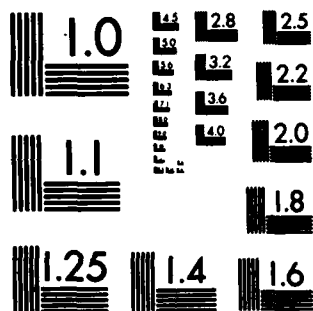
DEVELOPMENT OF A SILICON LIQUID-CRYSTAL LIGHT VALVE FOR 1/1
MULTIMODE OPERATION(U) HUGHES RESEARCH LABS MALIBU CA
U EFRON ET AL. JUL 82 N00024-78-C-5366

UNCLASSIFIED

F/G 20/12 NL



END
DATE
FILMED
83
DTIC



MICROCOPY RESOLUTION TEST CHART
NATIONAL BUREAU OF STANDARDS-1963-A

ADA 123 887

DEVELOPMENT OF A SILICON LIQUID-CRYSTAL
LIGHT VALVE FOR MULTIMODE OPERATION

U. Efron, E. Wiener-Avnear, J. Grinberg, P.O. Braatz,
M.J. Little, and R.N. Schwartz

Hughes Research Laboratories
3011 Malibu Canyon Road
Malibu, CA 90265

July 1982

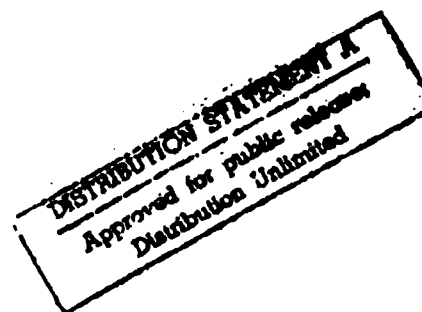
N00024-76-C-5366

Final Report: Phase II

1 January 1978 through 28 February 1982

Prepared For
DEPARTMENT OF THE NAVY
Naval Sea Systems Command
Washington, D.C. 20362

DTIC FILE COPY



83 01 28 036

UNCLASSIFIED

SECURITY CLASSIFICATION OF THIS PAGE (When Data Entered)

REPORT DOCUMENTATION PAGE		READ INSTRUCTIONS BEFORE COMPLETING FORM
1. REPORT NUMBER	2. GOVT ACCESSION NO.	3. RECIPIENT'S CATALOG NUMBER
	A123887	
4. TITLE (and Subtitle) DEVELOPMENT OF A SILICON LIQUID-CRYSTAL LIGHT VALVE FOR MULTIMODE OPERATION		5. TYPE OF REPORT & PERIOD COVERED Final Report, Phase II 1 Jan 78 - 28 Feb 1982
7. AUTHOR(s) U. Efron, E. Weiner-Avneer, J. Grinberg, P.O. Braatz, M.J. Little, and R.N. Schwartz		6. PERFORMING ORG. REPORT NUMBER
9. PERFORMING ORGANIZATION NAME AND ADDRESS Hughes Research Laboratories 3011 Malibu Canyon Road Malibu, CA 90265		8. CONTRACT OR GRANT NUMBER(s) N00024-76-C-5366
11. CONTROLLING OFFICE NAME AND ADDRESS Department of the Navy Naval Sea Systems Command Washington, D.C. 20362		10. PROGRAM ELEMENT, PROJECT, TASK AREA & WORK UNIT NUMBERS
14. MONITORING AGENCY NAME & ADDRESS (if different from Controlling Office) Naval Ocean Systems Center 271 Cataline Blvd. Bldg. A-33 San Diego, CA 92152		12. REPORT DATE July 1982
		13. NUMBER OF PAGES 85
		15. SECURITY CLASS. (of this report) UNCLASSIFIED
		15a. DECLASSIFICATION/DOWNGRADING SCHEDULE
16. DISTRIBUTION STATEMENT (of this Report) Approved for public release, distribution unlimited.		
17. DISTRIBUTION STATEMENT (of the abstract entered in Block 20, if different from Report)		
18. SUPPLEMENTARY NOTES		
19. KEY WORDS (Continue on reverse side if necessary and identify by block number) Liquid crystal, Light valve, Large screen displays, Silicon photo- conductor, MOS structure, Projection system, Spatial light modulator, Photoactivated liquid crystal light valve		
20. ABSTRACT (Continue on reverse side if necessary and identify by block number) The aim of this program has been to develop the silicon photoconductor liquid crystal light valve (LCLV) as a second-generation, higher- performance device, as well as to optimize the multimode operation of the liquid crystal. The latter effort was primarily aimed at allowing a full-performance CdS LCLV to be realized, given the switching-ratio limitation of this device, as well as to allow the silicon LCLV, when		

DD FORM 1473

1 JAN 73

EDITION OF 1 NOV 65 IS OBSOLETE

UNCLASSIFIED

SECURITY CLASSIFICATION OF THIS PAGE (When Data Entered)

UNCLASSIFIED

SECURITY CLASSIFICATION OF THIS PAGE(When Data Entered)

completed, to fully benefit from this development. This program has resulted in the successful development of a silicon LCLV in which we have solved the edge breakdown effect, developed a novel Si/SiO₂ dielectric mirror, implemented a focusing-grid to improve resolution and scaled up the device from a 1 cm x 1 cm aperture to a 2 in. aperture device. This has resulted in a fast-response, high switching-ratio device approaching the resolution performance of the CdS light valve. The LC multimode operation has been successfully optimized, resulting in a practical demonstration of a back-slope-type operation applicable to the switching-ratio-limited CdS devices. Results of the theoretical model developed for the liquid crystal operation were in good agreement with experimental measurements.

All results obtained from this theoretical study will directly benefit the silicon-based LCLV.

UNCLASSIFIED

SECURITY CLASSIFICATION OF THIS PAGE(When Data Entered)

TABLE OF CONTENTS

SECTION		PAGE
1	INTRODUCTION	7
2	DESCRIPTION OF THE SILICON LCLV	9
	A. General	9
	B. Device Operation	9
	C. Details	13
3	PROGRAM ACHIEVEMENTS	29
	A. Improvements in Silicon Processing Procedures	29
	B. The Development of Novel Thin-Film Structure	36
	C. Scale Up to 2 In.	36
	D. Solution of the Edge-Breakdown Problem	38
	E. Achievement of the Design Goals for Switching ratio, Resolution, and Time Response	41
	F. The Multimode Theoretical Program.	42
	G. Multimode Optimization and Back Slope Mode	60
4	DELIVERIES	67
	A. Silicon Light Valve Deliveries	67
	B. Multimode Liquid Crystal Cells	73
	C. Silicon Light Valve for Multimode Operation	
5	CONCLUSIONS AND FUTURE ISSUES	81
	ACKNOWLEDGEMENT	83
	REFERENCES	85

Accession-Per.	
NTIS GRA&I	<input checked="" type="checkbox"/>
DTIC TAB	<input type="checkbox"/>
Unannounced	<input type="checkbox"/>
Justification	
By	
Distribution/	
Availability Codes	
Dist	Avail and/or Special
A	



LIST OF ILLUSTRATIONS

FIGURE		PAGE
1	Schematic of the photoactivated silicon LCLV	10
2	Structure of the photoactivated silicon LCLV	11
3	Rotation of molecules in LC layer	18
4	Operation of the hybrid field effect mode in the on- and off-state	19
5	Calculated values for twist and tilt angles along with ideal values	20
6	Transmission versus voltage for the hybrid field effect	22
7	45°-twist HFE mode: liquid crystal thickness = 6.0 μm	23
8	Transmission characteristic of a 45° hybrid field effect mode cell at high voltage	24
9	Transmission versus voltage for hybrid and multimode field effect	25
10	Surface alignment for hybrid and multimode field effect	26
11	Imaging light activation of color graphics and symbology	27
12	Minority carrier generation lifetime of p-type Si substrates as a function of processing temperatures	32
13	The silicon liquid crystal light-valve assembly	38
14	Comparison of good CdS and 50 L/mm silicon light valve MTF characteristics	43
15	The silicon liquid crystal light valve response curve	44
16	LV response to input photopulse	45
17	Block diagram of the general computer approach for solving the electro-optic characteristics of the twisted nematic liquid crystal cell	47

FIGURE

PAGE

18	Perspective look at the twisted nematic liquid crystal realignment with maximum twist - W_m , used in the hybrid field mode of operation	49
19	Flow chart of the TILST computer program	50
20	The (a) tilt angle and (b) twist angle along the twisted nematic LC cell as computed by the TILST computer program for maximum twist angle 60° and E-7 type LC mixture - $1 < U/U_0 < 5.5$	52
21	Theoretical calculation of the tilt angle along the twisted nematic LC cell for $W_m = 45^\circ$ and $1 < U/U_0 < 5.5$	53
22	Theoretical calculation of the twist angle along the twisted nematic LC cell for $W_m = 45^\circ$ and $1 < U/U_0 < 5.5$	54
23	A schematic representation of the operation of the hybrid field effect mode	57
24	Flow chart of the HYBRIDEO computer program	59
25	Theoretical transmission characteristic curves for $L = 16$ microns thick and $W_m = 60^\circ$ twisted nematic cell	62
26	Measured transmission curves for LCLV H1765-21-D	63
27	Theoretical transmission characteristic curves computed for the BSM configuration of a $4.33 \mu m$ thick LCLV with maximum twist $W_m = 60^\circ$ and input polarizer angle $i = 30^\circ$	65
28	Measured transmission characteristic curves for multimode operation of BSM delivered liquid crystal cell	75
29	Measured transmission characteristic curves for BSM delivered liquid crystal cell	76
30	Theoretical transmission curves for the BSM configuration of a $5.4 \mu m$ thick LCLV with maximum twist $W_m = 70^\circ$ and input polarizer angle $i = 35^\circ$	77
31	Measured transmission characteristic curves for delivered CdS liquid crystal light valve, demonstrating multimode operation	79

SECTION 1

INTRODUCTION

The aim of this program has been to develop the silicon photoconductor liquid crystal light valve (LCLV) as a second-generation, higher-performance device, as well as to optimize the multimode operation of the liquid crystal. The latter effort was primarily aimed at allowing a full-performance CdS LCLV to be realized, given the switching-ratio limitation of this device, as well as to allow the silicon LCLV, when completed, to fully benefit from this development. The silicon photosensor, with its relatively small energy bandgap (1.1 eV), has several significant advantages over the wider bandgap CdS (2.4 eV). First, the much smaller bandgap width of the silicon implies negligibly small detrapping times for carriers and, thus, a very fast response to changes in the carrier density due to changes in the illumination level when compared to the CdS photosensor. Second, the silicon photosensor can be manufactured as a single crystal with an extremely low doping level. Hence, a wide depletion region can be set up, resulting in a very low dark current on the one hand and high sensitivity to illumination on the other. Switching ratios (illuminated to dark current ratios) of up to 20:1 are theoretically possible. It should be pointed out that a sufficiently high ($>3:1$) switching ratio is critical in achieving full multimode performance. Third, in the metal oxide semiconductor (MOS) configuration, the silicon photosensor is expected to result in a much higher linearity than the CdS-based LCLV. And fourth, the huge developments in the silicon industry will result in obvious benefits such as output uniformity (single crystal versus CdS polycrystal), well-developed standardized production, and cosmetic quality. It is thus obvious that the silicon LCLV, when developed, will supersede the CdS-based light valve in all respects and, in particular, in speed and switching ratio pertinent to the multimode operation. Preliminary experimentation with the silicon photosensor produced very encouraging results, thus demonstrating the feasibility of this idea. However, problems such as edge breakdown, inadequate mirror performance, and the capability of processing a 2-in.-diameter, 5-mil-thick wafer, had to be solved in order to demonstrate the practical use of silicon as the light valve photosensor. Answers to these

problems were provided conclusively by this program, which resulted in a full 2 in., fast-response, high switching-ratio device, approaching the resolution performance of the CdS light valve. The LC multimode operation has been successfully optimized, resulting in a practical demonstration of a back-slope-type operation applicable to the switching-ratio-limited CdS devices. Results of the theoretical model developed for the liquid crystal operation were in good agreement with experimental measurements as regards output intensity and color content of the LCLV in various cell configurations. Thus, the cell parameters (twist angle, thickness, and input polarization) were suitable for tailoring to the specific needs of the devices; in particular, a full three-color plus gray scale operation in a CdS device. All results obtained from this theoretical study will directly benefit the silicon-based LCLV.

SECTION 2

DESCRIPTION OF THE SILICON LCLV

A. GENERAL

The structure of the multimode silicon photoactivated LCLV consists of a silicon photosubstrate, thin-films, and an LC layer sandwiched between transparent counter electrodes deposited on thick glass baseplates (see Figures 1 and 2). The active device area is doped with a grid-structure microchannel stop that separates the individual resolution cells and defines the resolution of the device. The device is biased with an asymmetrical ac-type voltage. The voltage coupled onto the LC layer is controlled by the silicon photosensor, which is in turn activated by the image light.

Because of the wide spectral response of silicon, an effective wide-band light blocking layer (LBL), such as a cermet structure, must be used. The cermet structure consists of a sandwich of alternating thin layers of metal islands and dielectric films. Light blocking is achieved by absorption by the metallic islands embedded in the cermet. The combination of the LBL and the dielectric mirror (DM) enables independent writing and reading of the device without regard to the spectral response of the two light beams.

Hughes Research Laboratories (HRL) developed the hybrid twisted nematic effect liquid crystal used in the LCLV. In an ac field, the layer becomes birefringent and thereby rotates the polarization of light passed through it. The LCLV converts the input visual image into a voltage pattern across the LC and then into a polarizing image in the LC. The light valve is illuminated with polarized light which passes through the LC layer; this light is then reflected by the dielectric mirror and passes back through the LC. A polarizer external to the LCLV selects the polarized image light for projection.

B. DEVICE OPERATION

The voltage waveform applied to the silicon-LCLV is also shown in Figure 2. It is composed of assymetric periodic depletion-accumulation phases. During the main depletion phase (positive voltage on counter electrode for n -type silicon), the n substrate is fully depleted along with a

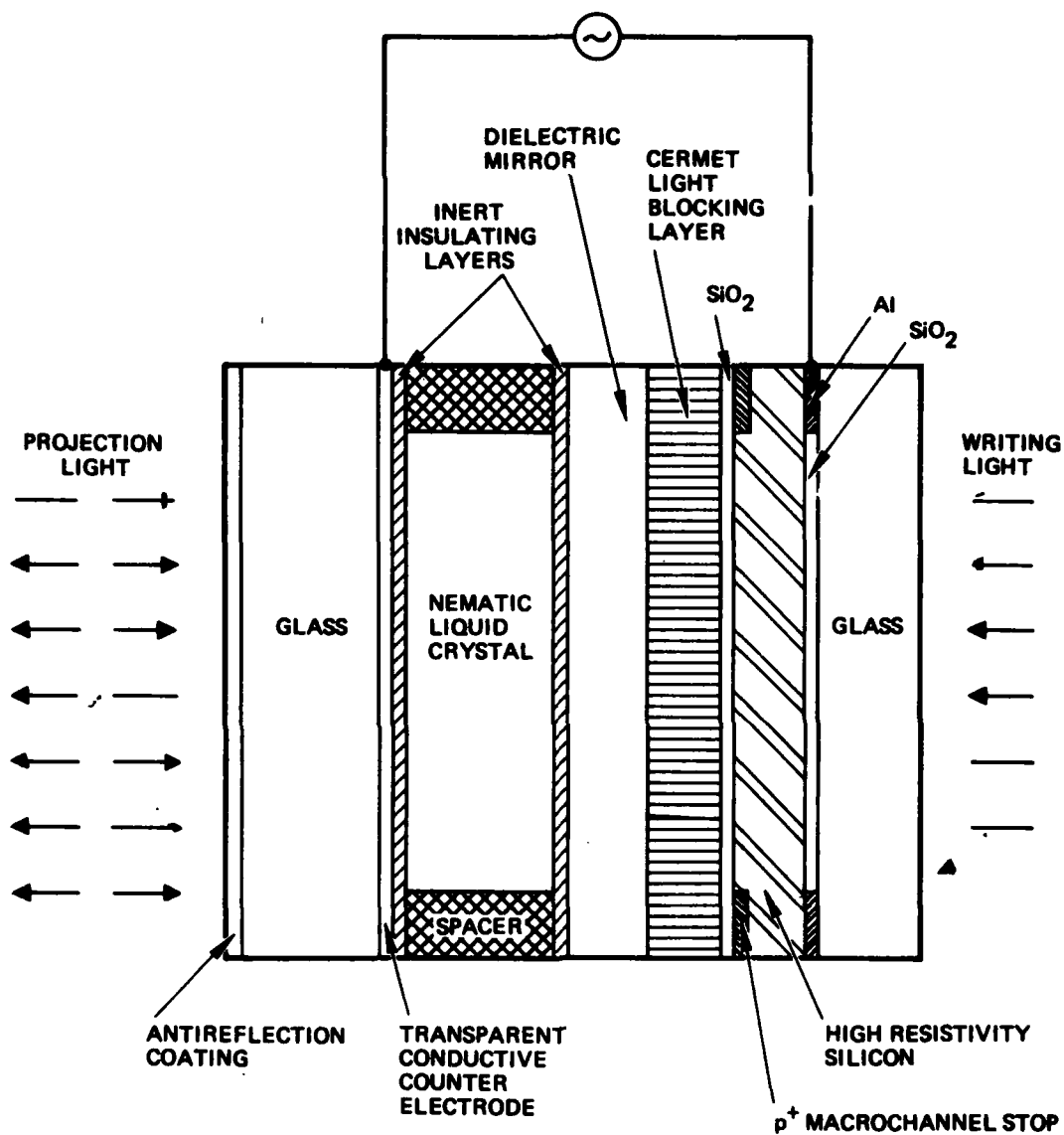


Figure 1. Schematic of the photoactivated silicon LCLV.

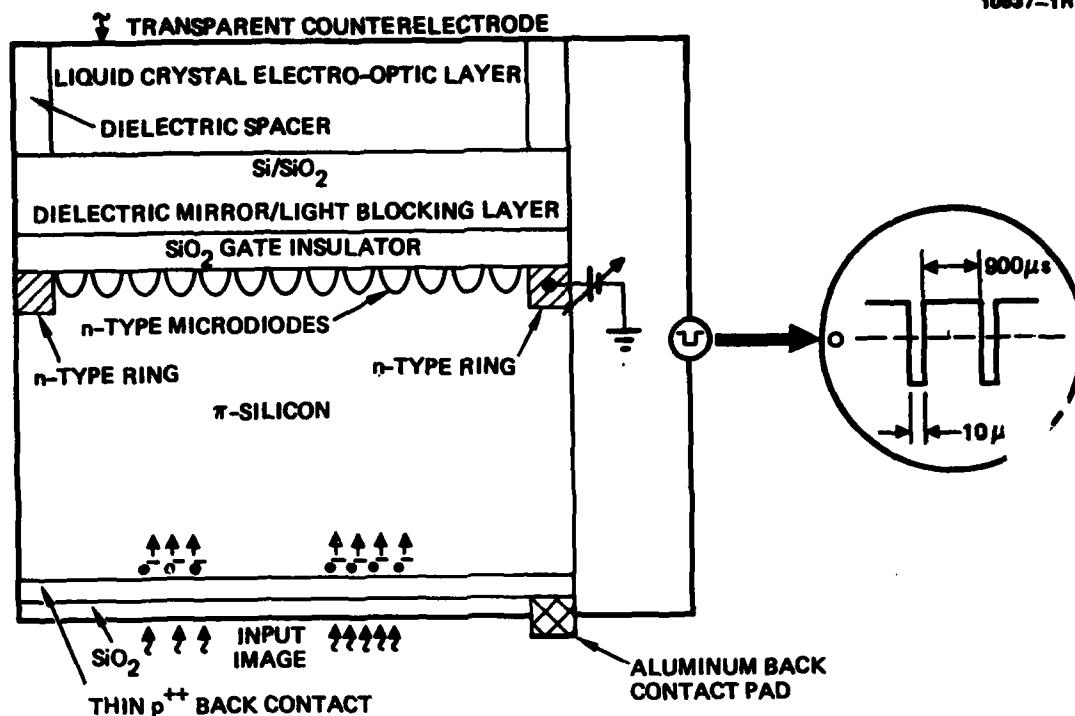


Figure 2. Structure of the photoactivated silicon LCLV.

portion of the heavily doped p^+ back contact. Thus, the electron-hole pairs created by the incoming photons are drifted by the electric field existing in the depleted region. Holes are drifted to the back-contact area, and electrons are drifted to the Si/SiO_2 interface, where they finally reside. The current loop is completed by the passage of a positive charge through the LC to balance the electron charge at the Si/SiO_2 interface. Thus, a spatial pattern of signal current or voltage drop on the liquid crystal exists in proportion to the spatial input light pattern (i.e., according to the input image). This voltage pattern is converted into a spatial birefringence pattern on the LC, which in turn spatially modulates the rotational degree of the readout beam's polarization. The physical arrangement to observe this spatial polarization modulation is as follows: (1) The readout beam enters the LC layer and then passes through the LC again as it is reflected from the dielectric mirror; then (2) the readout beam is cross-polarized as it emerges from the LC. Combining this sequence of operations, it then follows that the spatial pattern of output light intensity is proportional to the input image.

As noted above, the signal electrons generated by the input optical signal residing at the Si/SiO₂ interface. These are "erased" periodically by the accumulation or refresh phase. During this short-duration phase (negative voltage applied to the counter electrode), electrons are pushed into the π substrate and are recombined with the injected holes. However, during the depletion phase, a sufficiently high light intensity will generate a high density of electrons at the Si/SiO₂ interface which may result in a partial collapse of the depletion region. This will also lead to the migration of the electron charges across the equipotential Si/SiO₂ interface, causing the resolution to degrade. The partial collapse of the depletion region is detrimental to device performance in that signal electrons created in the depletion-collapsed region will have to diffuse through this region and thus sustain both recombination losses and diffusion spreading. These will result in sensitivity and resolution degradation. Also, since the sensitivity will now be dependent on input light level (through the degree of depletion region collapse), the device will exhibit nonlinear transfer characteristics. To avoid these effects, two features have been incorporated into the Si LCLV structure: a heavily doped p⁺ back contact and a focusing grid. The back contact is partially depleted (along with the π substrate) during the depletion phase. Thus, it will sustain the depletion collapse caused by the signal electrons that have drifted from the Si/SiO₂ interface and hence allow the π region to remain in total depletion. The focusing microgrid (to be detailed later) acts to create potential wells for the electrons at the Si/SiO₂ interface. Incoming electrons will then be focused into buckets at these wells, thus avoiding their spreading and the associated resolution losses. Obviously, this grid now determines the limiting resolution of the device (assuming that all other resolution losses are negligible). We have, therefore, the practical advantage of controlling the device resolution by changing the grid geometry. Finally, to avoid the injection of carriers from the device periphery into the active area, some means of edge protection must be incorporated. The final solution to this problem has been found to be the dc-biased guard ring, shown in Figure 2. This ring creates an infinite sink to laterally injected electrons, thus completely eliminating the edge-6

C. DETAILS

1. Silicon Photo Substrate

The starting material is a high-resistivity (5 to 8 $\text{k}\Omega\text{-cm}$) single crystal $\langle 100 \rangle$ with a high minority carrier lifetime (1000 μsec or better). A float-zone-type crystal is preferred due to its higher purity and low oxygen content. The reason for selecting a 5-mil-thick substrate with high resistivity is based primarily on the impedance required. Thus, to match the impedance of a 12- μm -thick LC cell with $\epsilon \approx 12$ (i.e., $C_{\text{LC}} \approx 0.9 \text{ nF/cm}^2$) will require $C_{\text{Si}} = C_{\text{LC}}/9 = 0.1 \text{ nF/cm}^2$ to achieve a switching ratio of about 10:1. This corresponds to a depletion width of about 100 μm , thus determining the thickness of the substrate. Doping level is then determined by the requirement to fully deplete the MOS structure with a reasonably low ($\sim 25 \text{ V}$) voltage. This corresponds to a doping level of about $2 \times 10^{12} \text{ A/cm}^3$, or about 8 $\text{k}\Omega\text{-cm}$ π -type silicon.

a. The π -p Focusing Grid

As explained above, a structure consisting of potential wells for the signal electrons is required at the Si/SiO₂ interface in order to confine these charges to well defined "buckets" and prevent their lateral spread and the subsequent loss of resolution. The π -p focusing grid developed utilizes a set of p-type grid lines to realize the barriers required to isolate the individual resolution elements. This potential variation results from the concentration gradient existing between the high-resistivity (π) Si cells and the boron-doped grid lines, and from the thermodynamic requirement for the Fermi levels in the respective regions to align in thermal equilibrium. Hence the signal charge packets reside in the potential wells between the grid lines, and are prevented from spreading to neighboring cells by these electrostatic barriers.

In normal operation the depletion voltage (positive with respect to the substrate/epilayer) is applied simultaneously to both the π region and the grid lines. Since the grid lines are much more highly doped than the π substrate, the magnitude of the depletion voltage is chosen to fully deplete the substrate to the p^+ boundary under these highly doped grid lines. Thus, the

minority-carrier signal charge is transported and collected in the π regions where it is stored for the full frame time until the applied voltage is periodically reduced to zero. During this short accumulation time, the respective depletion regions collapse, and majority carrier holes are injected through the p^+ Ohmic back contact into the substrate where they recombine with the signal charge. This process effectively resets the frame of information so that a new charge pattern can be formed by the input image at the termination of the accumulation pulse period.

b. The p^+ Macro-channel Stop

The heavily doped p^+ macro-channel stop on the periphery of the active area functions to isolate the main array from the deleterious effects of thermal generation occurring at the sides of the device. Some of these edge-generated minority carriers, which travel by random thermal diffusion, eventually get scattered into the p^+ macro-channel stop volume where they combine with the much more highly concentrated majority carrier holes. Unfortunately, those carriers that do not recombine in the macro-channel stop are now available to recombine in the high-resistivity, undepleted, bulk regions where the electron diffusion length is much longer. Since the thermal-generated minority carriers can travel over much greater distances in the undepleted π bulk regions, it is very likely that these carriers will be collected by the active region MOS capacitors where they will contribute to the overall dark current and thereby reduce sensitivity.

2. Wafer Polishing

Wafer thin-down and double-sided polishing are required to obtain the final 5-mil-thick wafers for the subsequent MOS processing. Since flatness uniformity is a determining factor in LV output uniformity, special care must be exercised during polishing to avoid warpage or "dimples" in the wafer. Small (few fringes) final warpage may be tolerated if the thickness uniformity has been preserved. This is so because the wafer can be "flattened" during the mounting stage. Warpage is usually due to the use of: (1) thick, high-melting-point mounting wax or (2) a relatively low starting wafer thickness (10 mils or less) or their combination. Dimples are associated with the degree of cleanliness of the polishing facility and of the mounting wax. The

use of low-melting thin wax will, in general, lessen wafer warpage but will tend to promote dimple formation.

3. Silicon Processing

The "end product" is the MOS structure with grid implantation at the Si/SiO₂ interface to preserve spatial resolution of the signal charge pattern residing at this interface. The processing involves:

- Macro-channel stop and back contact (p⁺) implantation/diffusion. The first is required to protect against edge injection (see later discussion); the latter is required to establish a contact to the silicon substrate.
- Implantation of the microgrid for the signal charge focusing discussed above.
- Gate oxidation. This results in a high-quality thermal oxide to serve for the MOS operation and to block passage of dc current through the device.
- Metalization.

The most critical stages are the field/gate oxidation and diffusions since these involve high-temperature (>900°C) processing. Some damage to the silicon lattice is unavoidable, resulting in loss of minority carrier lifetime. The low doping level should be retained by guarding against contamination in the various processing stages. The retention of a relatively high minority-carrier lifetime is essential in keeping the MOS structure in full depletion during the active phase as well as in avoiding high dark current. Failure to retain the substrate at full depletion will degrade the resolution, sensitivity, and linear response of the device. The resolution loss will occur because the signal charge in the partially collapsed substrate (due to high thermal generation) will have to diffuse through a partially collapsed substrate, as opposed to drifting by the electric field in a well-depleted substrate. Sensitivity will be affected by recombination losses of the signal charge while diffusing through the partially collapsed region. Linearity of response is affected since, in a partially collapsed substrate, any subsequent photoinjection will lead to a further collapse of the depletion region and to partial recombination of the photocarriers. Thus, input

illumination will result in decreasing photo-current generation, making the device response nonlinear. Similarly, an increase in the very low doping level will result in the inability to fully deplete the substrate at normal voltages, leading to consequences as described above.

4. Thin-Film Structure: Light Blocking Layer (LBL) and Dielectric Mirror (DM)

The DM should feature: high (>90%) reflectivity (to accomplish high contrast and avoid substrate heating by absorption at the high readout light level required); sheet resistivity of $10^{12} \Omega/$ or better; annealability at up to 500°C; and chemical inertness, with respect to the LC. The high sheet resistivity is required to maintain a well-defined voltage pattern across the device. Annealability is essential to reduce the damage to the silicon substrate caused by the stress from the evaporated film as well as from x-ray exposure. Similarly, the requirements of the LBL are annealability, high sheet resistivity, and a high degree of optical isolation (> 10^6), particularly important in the silicon device (as compared to the CdS device) due to the high broadband photo-sensitivity of the silicon photosubstrate. In addition, the LBL should be relatively specular so as to avoid subsequent non-specularity and thereby diminish appreciable scattering of the overlaid mirror.

5. Liquid Crystal

This serves as the light modulator by means of polarization rotation and the subsequent use of an analyzer. The silicon light valve, like the CdS light valve, is an ac device with the LC in the twisted nematic configuration operating in the hybrid field effect mode. Its operation is described in detail below.

The LC molecules at the electrodes are aligned with their long axes parallel to the electrode surfaces. In addition, they are aligned to lie parallel to each other along a preferred direction that is fabricated into the device. The twisted alignment configuration is obtained by orienting the two electrodes so that the directions of LC alignment on the two electrode surfaces make an acute (or right) angle with respect to each other. As a

result, as shown in Figure 3, molecules in the bulk of the LC layer rotate through this angle in traversing the space between the electrodes. This twisted alignment configuration, combined with the intrinsic optical birefringence of the LC, causes the polarization direction of linearly polarized incident light to rotate exactly through the twist angle. This is the so-called twisted nematic effect. In conventional twisted nematic devices, the twist angle is 90° . As described below, in the device under discussion here, we twist the molecules through 45° .

To understand the operation of the hybrid field effect mode, first consider the off-state. As shown in Figure 4, we place a crossed polarizer/analyzer pair between the light valve and the read-out light source. The polarizer is placed in the incident beam and the analyzer is placed in the reflected beam. This provides a dark off-state because after its first pass through the LC layer the direction of polarization of the linearly polarized incident light is rotated through 45° . But upon reflection from the DM, the light passes a second time through the LC and its polarization is rotated back to the direction of the incident light where it is blocked by the crossed analyzer. Thus, the off-state of the device is determined entirely by the twisted nematic effect.

In the on-state, we apply a voltage and rotate the molecules to the homeotropic alignment.* For the case of "perfect" homeotropic alignment, however, the polarization of the light would not be affected by the LC and we would have a dark on-state as well. This would be of no value. Closer scrutiny of the process whereby the molecules untwist, however, shows that between full "off" and full "on" there exists a voltage regime where the device will transmit light. As the voltage is applied to the LC the molecules begin to tilt toward the homeotropic alignment (see Figure 4(b)). In this orientation of the molecules, between parallel and perpendicular, the optical birefringence of the molecules can affect the polarization of the light. As a result, at these intermediate voltages the light that emerges from the device after reflection from the mirror is no longer linearly polarized, so that some transmission can occur. The question is, how much? To answer this question,

*Alignment in which the long axis of the molecules is oriented perpendicular to the electrode surface.

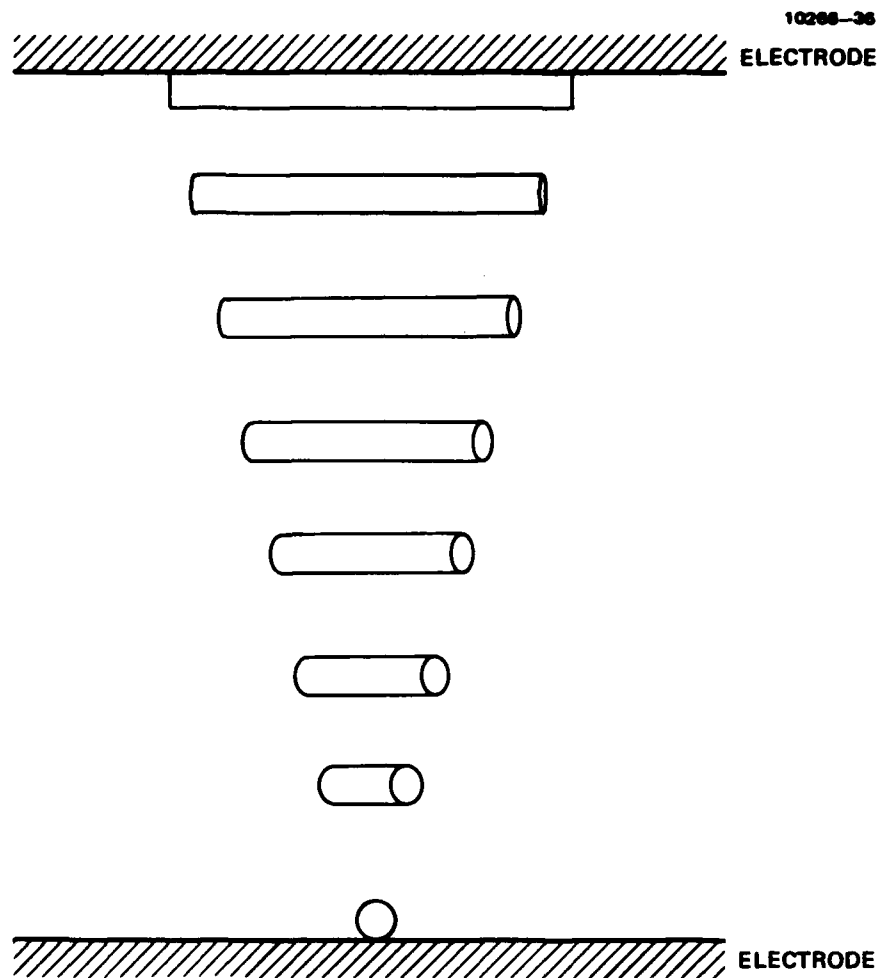
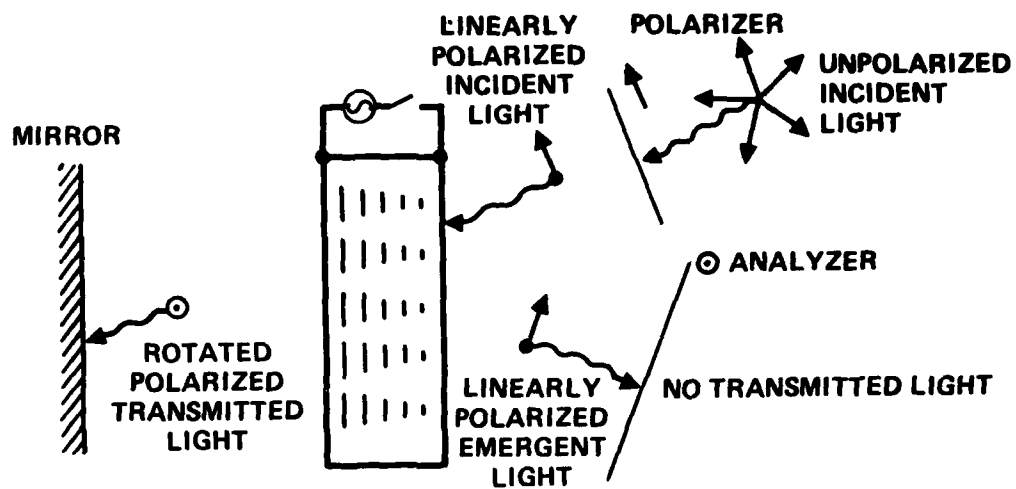
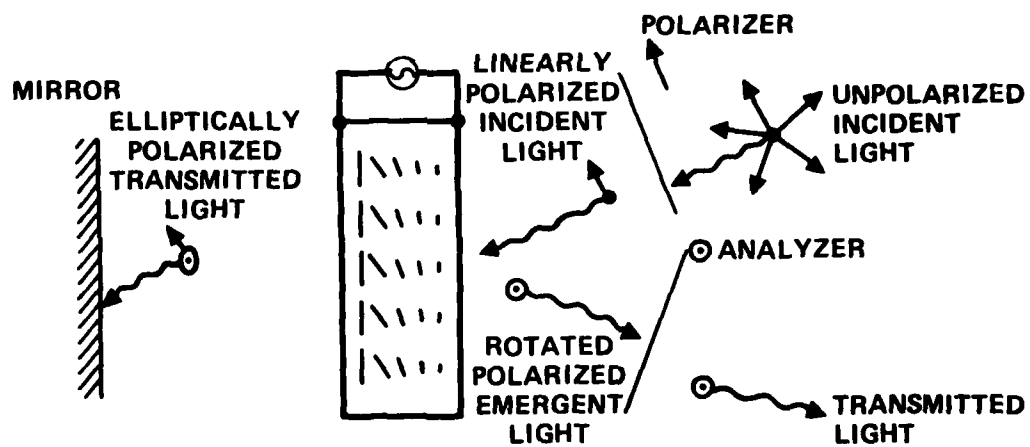


Figure 3. Rotation of molecules in LC layer.



a) OFF-STATE



b) ON-STATE

Figure 4. Operation of the hybrid field effect mode in the on- and off-state.

let us consider the orientation of the molecules as a function of position across the layer, with voltage applied to the device. Figure 5 shows calculated values¹ for the twist angle and for the tilt angle of the molecules as a function of position within the LC layer for a twisted alignment configuration device. As shown in Figure 5(a) the effect of the voltage is to destroy the twist spiral. In the ideal case, with the voltage on, half of the molecules in the layer adopt the preferred alignment direction associated with one electrode, and the other half adopt the alignment direction associated with the other electrode.

There is a realizable voltage regime in which the practical twist angle distribution of a twisted nematic device is close to this ideal distribution. The physical explanation for this behavior is as follows.

The twist of the molecules is transmitted from layer to layer by means of "long" range intermolecular interaction forces that are inherent in the LC. Generally speaking, as the tilt angle of the molecules grows (towards the perpendicular), the transmittance of the twist, from layer to layer, becomes less effective. If any layer has molecules aligned perpendicular to the electrodes, the transmittance of the twist by that layer goes to zero. This has

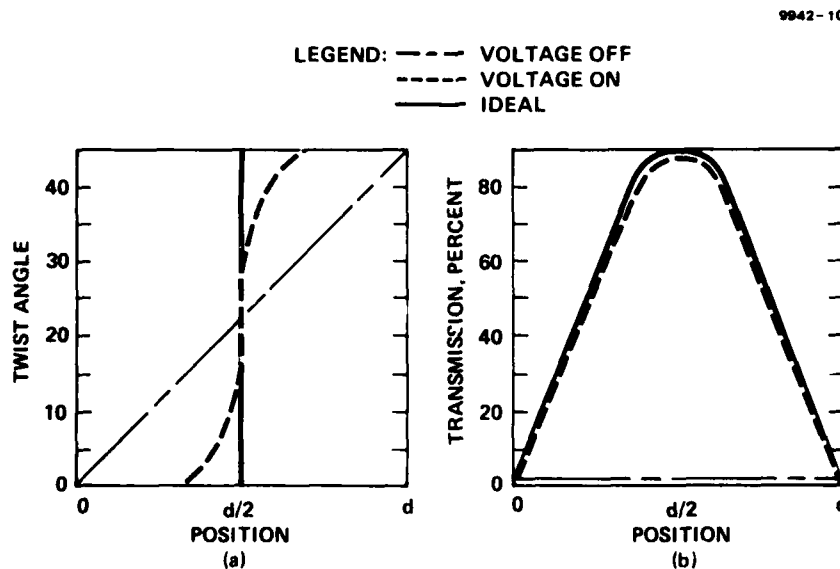


Figure 5. Calculated values for twist (a) and tile (b) angles, along with ideal values.

the effect of cutting the entire twist spiral into two separate parts. When this happens, the molecules snap into an alignment orientation that is determined by the closest electrode. This in turn causes the twist angle distribution to transform to the ideal one (Figure 5(a)). The foregoing describes the nature of the twist mechanism. Next, consider the effect of the voltage on the twist of an actual device.

The calculated tilt angle (θ) as a function of position along the cell thickness is shown in Figure 5(b). Close to the electrodes, the tilt angle is small; but at the center of the layer, it is large, because there the influence of the electrodes on the alignment of the molecules is at a minimum. For voltages that are just twice the threshold voltage, the tilt angle at the center of the cell is already 80° . Thus, with relatively low voltages switched to the LC, the spiral can be snapped and the distribution of twist angle will be close to the ideal shown in Figure 5(b). Moreover, in this near-ideal state the average tilt angle is much less than 90° . The device takes advantage of the birefringence of this state in the following manner.

The polarization of the light entering the device must be aligned along the preferred alignment direction of the entrance electrode in order to make the twisted nematic off-state work. Thus, when the molecules untwist, the polarization of the light would be 0° or at 90° (in a 90° twist-cell) with respect to the extra-ordinary axis of the LC throughout half of the layer. This optimizes the transmission of the device.

Figure 6 shows a plot of transmission versus voltage for the hybrid field effect. The two curves correspond to twist angles of 90° and 45° , respectively, between the preferred directions on the electrodes. The data were taken with 2- μ m-thick, reflection-mode cells filled with an ester nematic LC.

The polarizer was oriented parallel to the LC optical axis on the front electrode, and the analyzer was oriented perpendicular to the polarizer. The read-out beam was a He-Ne laser. As expected from the above reasoning, the birefringence of the 45° cell is considerably stronger than that of the 90° cell so that the maximum transmission for the 45° cell is much larger than for the 90° cell.

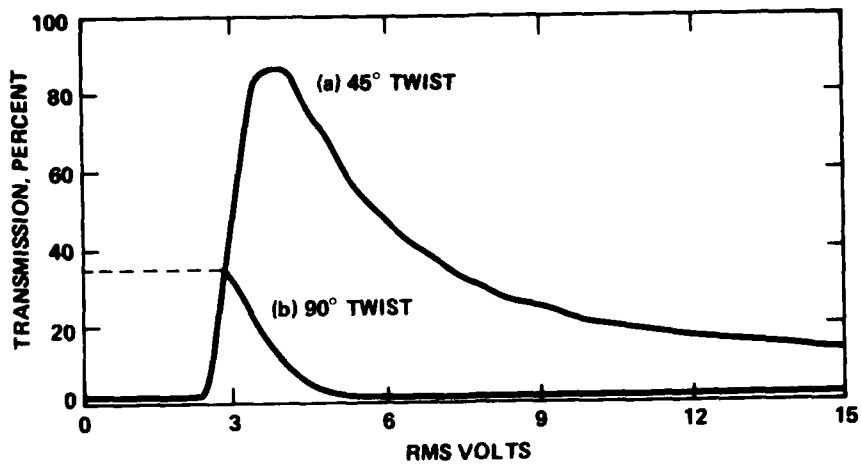


Figure 6. Transmission versus voltage for the hybrid field effect.

6. Liquid-Crystal Multimode Operation

"Multimode operation" is the LCLV operation by which color alphanumerics may be superposed on the regular gray scale projection. As explained in the introduction, the main effort of this program phase has been to achieve multimode operation. Thus, LC studies in this phase were devoted towards defining, both theoretically and experimentally, the LC cell parameters that will result in the achievement of a high-contrast, multicolor response at the relatively narrow switching ratio range ($\sim 2.5:1$) available in the CdS device. Results of these studies are, of course, directly applicable to the silicon LCLV.

Section 3F describes these studies and presents their results. At this point, we briefly describe multimode operation and its implementation in the silicon LCLV.

This mode of operation is based on utilizing the distinct color region of the transmission voltage curve (Figure 7) simultaneously with the black/white region. Thus, in a light valve biased at the null point of Figure 7, the successive colors would appear as indicated as the input light level is increased. As shown, this would be followed by a "white" peak and then a slow decrease to zero (dark state). Obviously, then, a true gray scale can only be

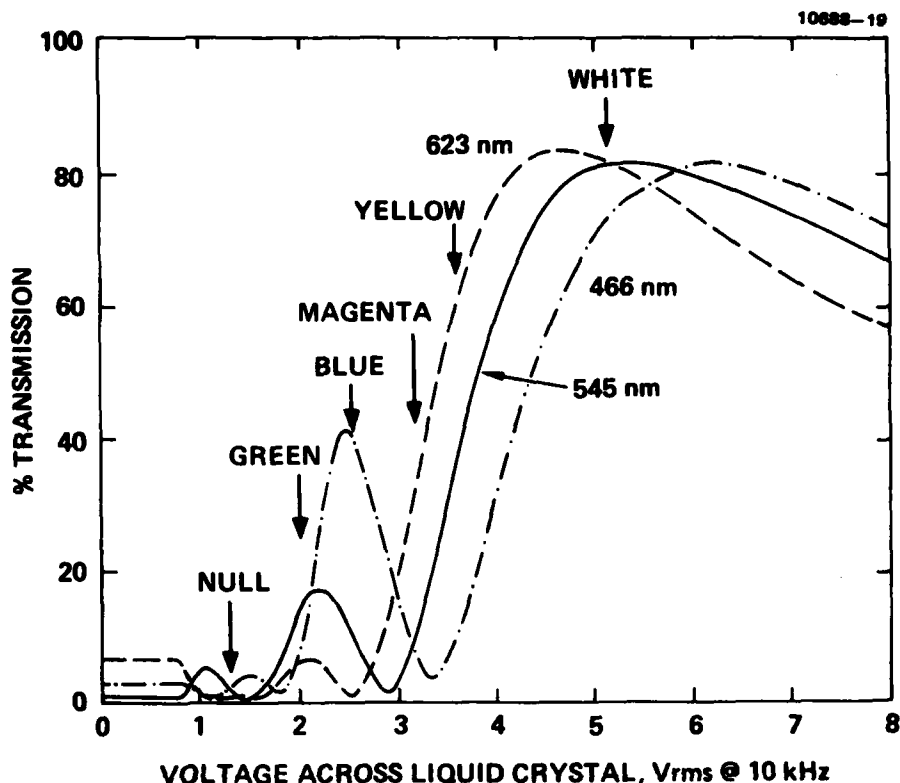


Figure 7. 45°-twist HFE mode: liquid crystal thickness = 6.0 μm .

obtained in the back-slope region ($V_{rms} < 4$ V). However, as Figure 8 shows, back-slope gray-scale operation with the color region included would require a switching ratio in excess of 15:1 (30 V:2 V) which is even beyond the capabilities of the Si-doped LCLV. This problem has been overcome by developing a multimode field-effect operation in which the back-slope region shrinks considerably so that a switching ratio of 2.5:1 is sufficient to cover both the color peaks and the gray-scale region. This is shown in Figure 9. The required changes in the twist angle, as well as in the incoming light polarization angle, are depicted in Figure 10. Multimode operation, then, consists of biasing the device in the front-slope null point (near the LC

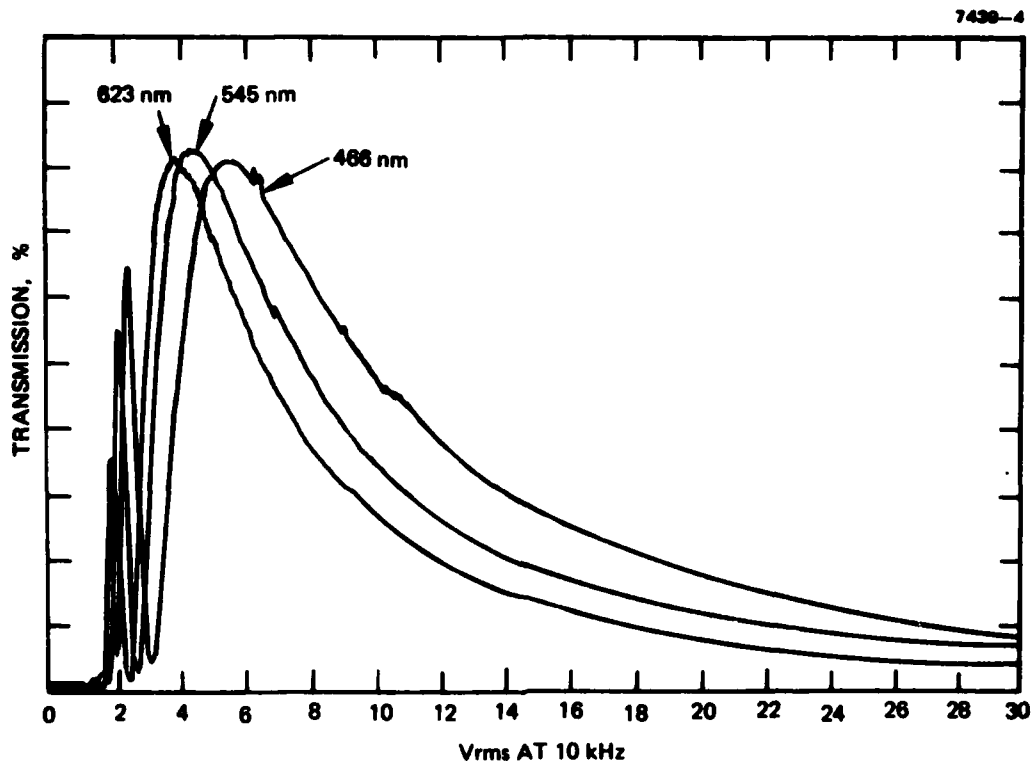


Figure 8. Transmission characteristic of a 45° hybrid field effect mode cell at high voltage.

threshold; see Figure 9.) In this way, the low intensity input light range (corresponding to low applied voltages on the LC) will be used for the color symbology. The high intensity light will then be used for the gray-scale projection (Figure 11), where the video level will be inverted. Since the "dc" brightness of CRT screens is adjustable and polarity reversal is a standard feature, this operating mode can be realized using standard CRT systems. The method obviously is applicable to the Si device since the switching ratio expected is in excess of 5:1. To implement this mode in the Si LCLV simply requires using a larger twist angle (typically 60°) and orienting the light valve with respect to the polarization of the incoming beam, as shown in Figure 10.

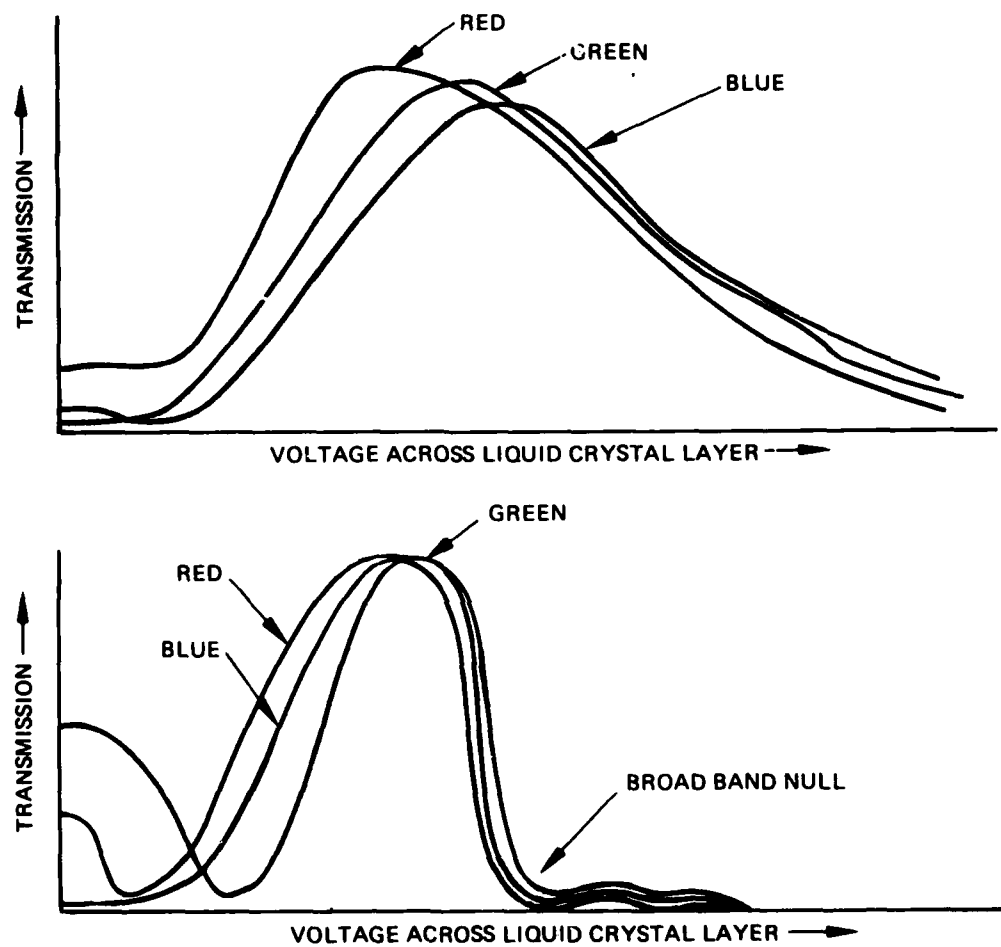


Figure 9. Transmission versus voltage for hybrid and multimode field effect.

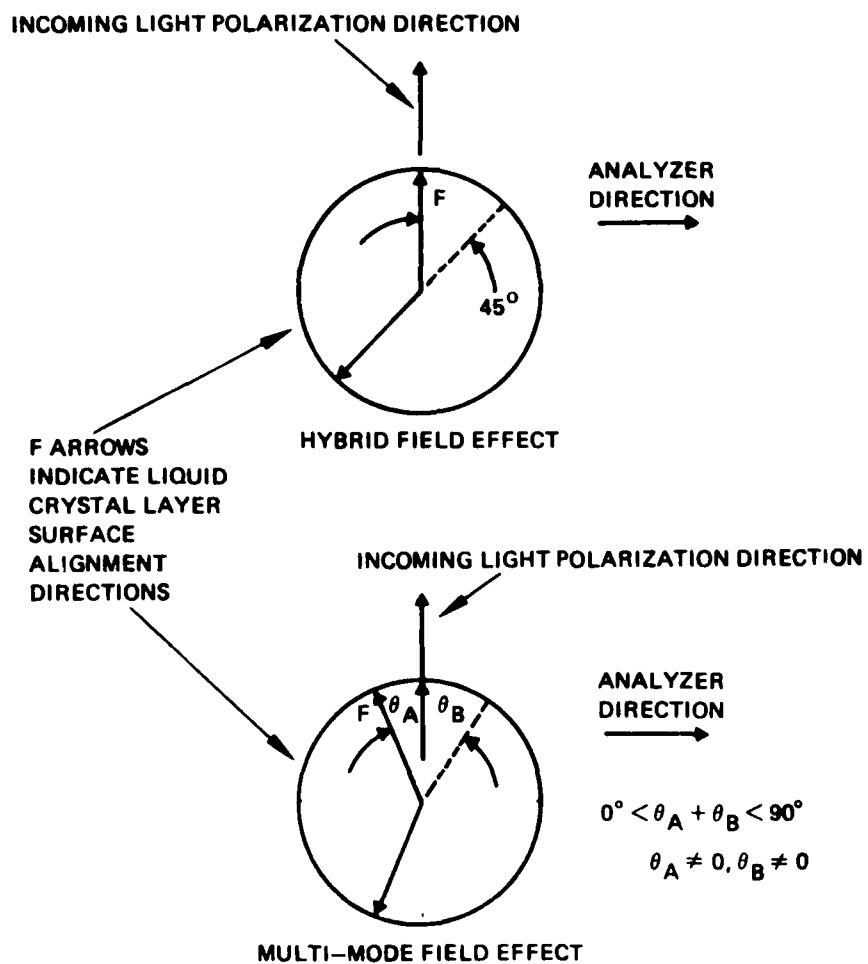


Figure 10. Surface alignment for hybrid and multimode field effect.

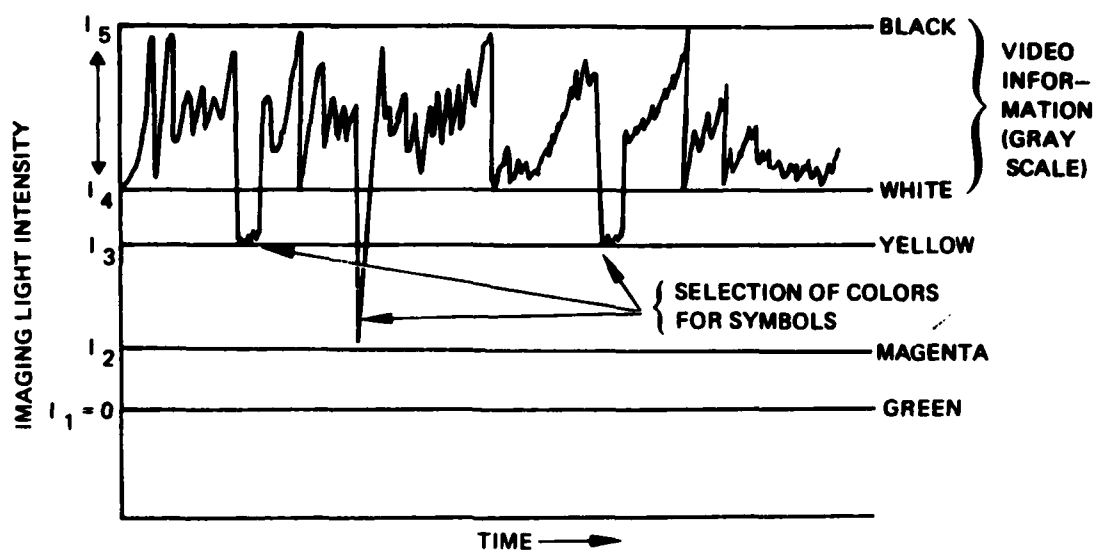


Figure 11. Imaging light activation of color graphics and symbology.

still under study due to difficulties with the wax dilution procedure. Good preliminary results were obtained showing a much smaller number of local defects in the polished wafer.

Turning now to the actual Si processing, a series of experiments aimed at evaluating the degradation incurred by the photosubstrate from the high-temperature cycles were carried out.² These experiments, performed both at the diffusion and the gate oxidation steps, clearly indicated the need to lower the processing temperature. Graphs of these results are shown in Figure 12. Following these conclusions, oxidation and diffusion temperatures were lowered to 925°C from an initial 1000°C. This led to a substantial gain in minority-carrier lifetime. Since large thermal gradient and thermal shocks are known to produce defects in silicon, we have implemented a slow push/slow pull technique at the gate oxidation and field oxidation steps to further reduce lifetime degradation. We have also implemented an HCL gettering procedure within the gate oxidation step. This causes volatile metal-chlorine compounds to form, thus eliminating metallic impurities in the oxide growth. This has the advantages of: (1) eliminating generation-recombination center of fast diffusers (such as copper or gold) and (2) creating a metal-free oxide that reduces flatband shifts and inhibits the surface inversion effect. As explained in Section 2, the micro-grid (or micro-channel grid) structure at the Si/SiO₂ interface offers the advantages of (1) creating a lateral focusing field for signal electrons created within the depletion region, and (2) creating a potential well at the Si/SiO₂ interface which prevents signal charge from spreading laterally. Such spreading would "smear" the image. We initially experimented with the π -p grid detailed in the preceding section. However, a new structure consisting of n-diode islands embedded in the native π channels proved superior experimentally. This structure, shown in Figure 2, is formed by implanting n-type square regions into the π -silicon. Thus, a microgrid structure is formed in which the dimensions of the cell control the limiting spatial resolution of the device. The combined n- π structure operates as follows. On depletion (gate positive with respect to substrate), the π -n junction is depleted, creating an active depleted π region for photocharge generation. The MOS structure formed by the oxide and the n-islands is forward biased in the "depletion" phase, enabling most of the voltage applied to drop on the n- π junction. The adjacent π channels are depleted by virtue

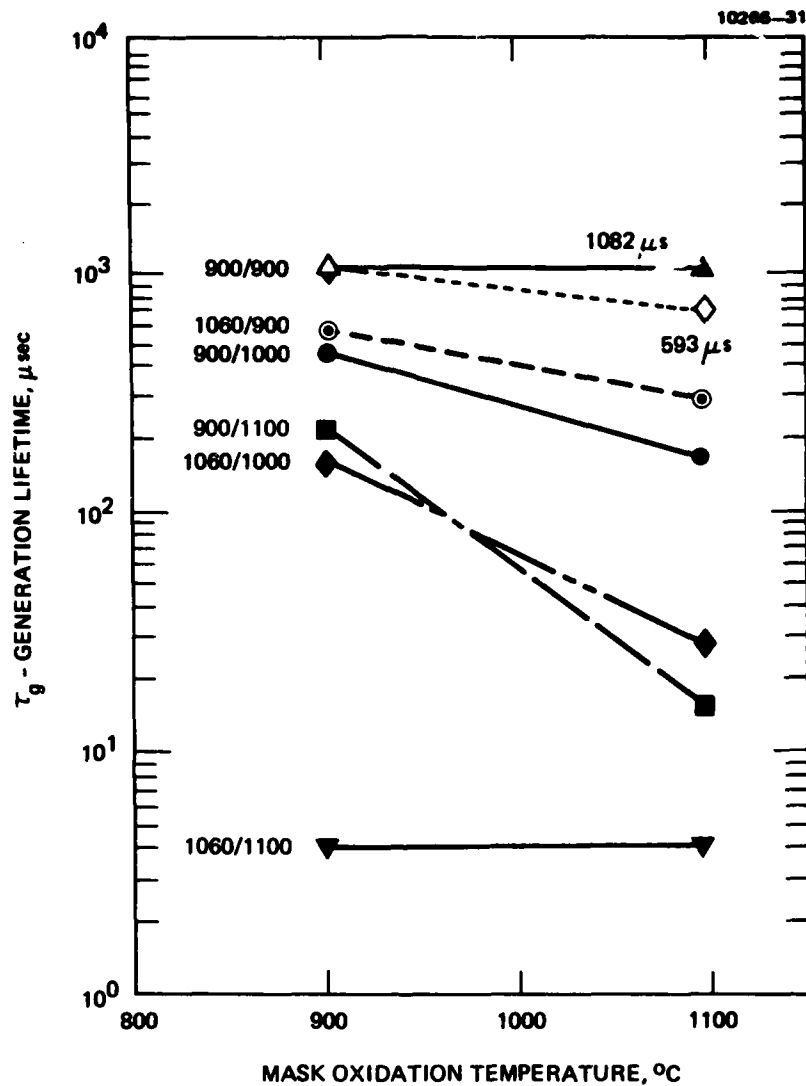


Figure 12. Minority carrier generation lifetime of p-type Si substrates as a function of processing temperatures.

- (a) Lifetime versus mask oxidation temperature
The channel stop diffusion/gate oxidation temperature are indicated.

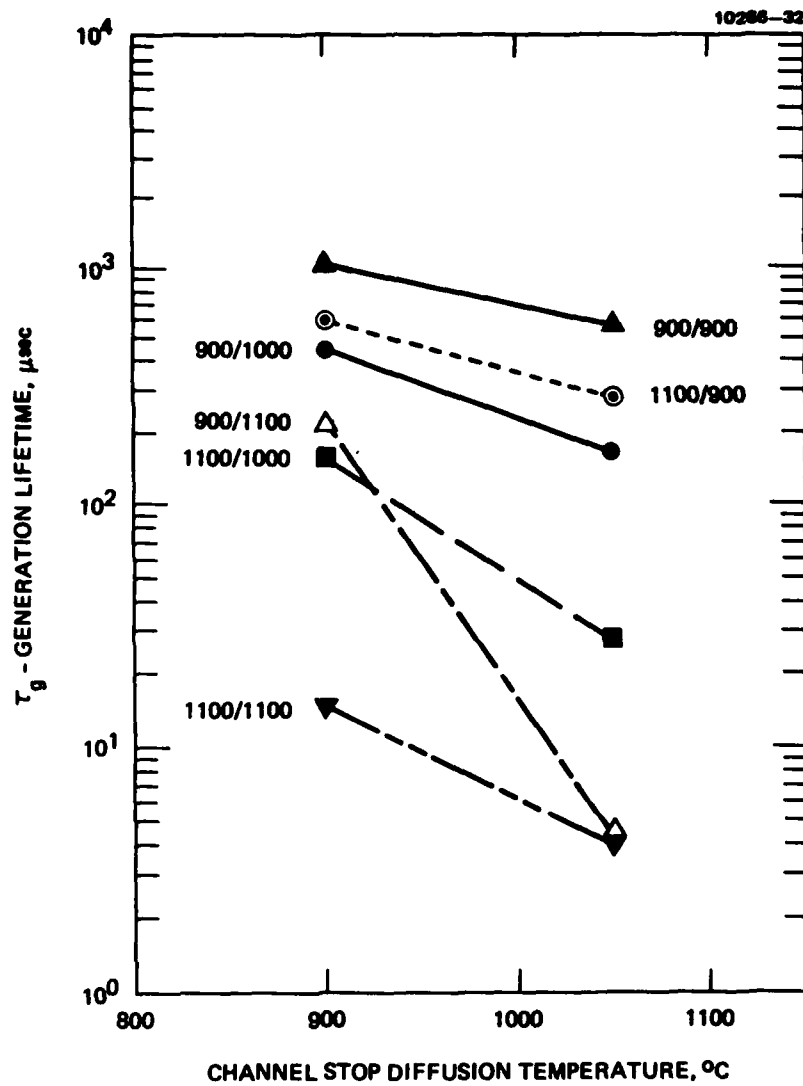


Figure 12. Continued

- (b) Lifetime versus channel stop diffusion temperature. The mask/gate oxidation temperatures are indicated.

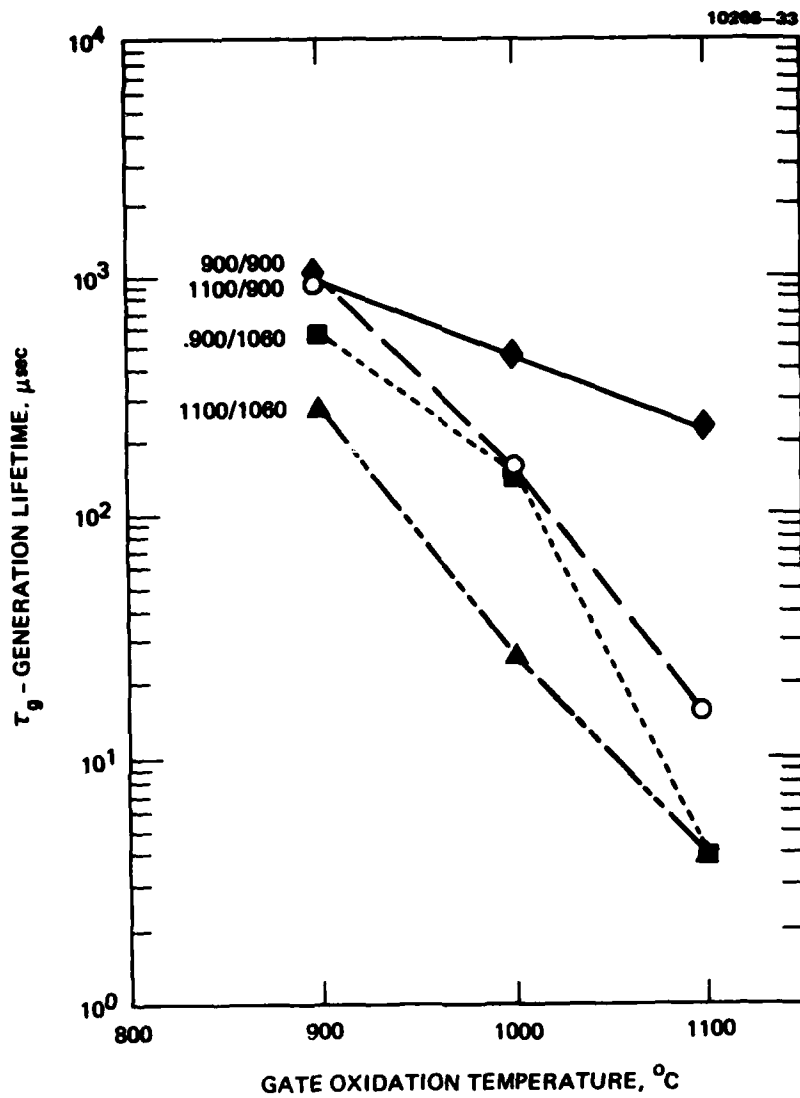


Figure 12. Continued

(c) Lifetime versus gate oxidation. The mask oxidation/channel stop diffusion temperatures are indicated.

of their MOS structure. By reversing the applied voltage to the short accumulation phase (gate negative with respect to substrate), the n-Si/SiO₂ junction will be driven into depletion, pushing the photo- and thermally-generated signal electrons into the π region where the n- π junction is now forward biased. Thus, the necessary recombination of the signal electron will take place (as in the "old type" π -p grid), which is essential in achieving the periodic frame-erasure. However, in contrast to the π -p grid structure during the depletion phase, use is made of the accumulation voltage that is dropped on the oxide and the depleted n region. This voltage is now used in creating a potential difference between the n region and the adjacent π channel. Thus, signal electrons are focused into charge buckets within the n islands to retain an unsmeared spatial charge pattern. A lateral focusing field for incoming signal electrons would exist even without the employment of the accumulation voltage. Thus, one advantage of this grid structure over the π -p structure is a significantly higher focusing potential for the signal electrons. A second advantage is that the focusing effect can now be controlled by adjusting the accumulation pulse level. A third advantage is a reduction in noise level. This is due to the additional depletion voltage that is required in the π -p grid case to deplete the extra charge in the p-implanted region. This results in higher transition current spikes and thus leads to a higher noise level. As explained in the n- π grid case, the accumulation voltage is effectively utilized in depleting the π region. Hence, a smaller voltage amplitude will be required with consequent reduction in the transition current spikes. One possible disadvantage of the n- π grid structure may be a lower efficiency in signal electron recombination. In the π -p grid case, the signal electrons are recombined at the Si/SiO₂ surface where they are momentarily trapped. Thus, during the transition to the accumulation phase, a high-density layer of holes (accumulated layer) is available for the surface recombination of electrons. In the n- π structure, assuming negligible trapping at the n- π interface, electrons will be ejected to the collapsed π region which has a relatively small density of holes available for electron recombination. Note again that we found the π -n structure to be superior to the π -p grid structure. Thus, we invested considerable effort in optimizing the n-implantation dose. This led to the dose implantation levels of $5 \times 10^{12}/\text{cm}^2$ and 1×10^{12} at 150 keV for the 33 and 50 line/mm grids, respectively.

B. THE DEVELOPMENT OF A NOVEL THIN-FILM STRUCTURE

The main requirements of the thin-film LBL and DM are high optical isolation ($>10^4$ -LBL), high reflectivity ($R > 0.9$)-DM, high sheet resistivity ($>10^{12} \Omega/\square$ -LBL and DM), the capability to withstand a high anneal temperature (450°C), chemical inertness with respect to the liquid crystal (DM), simplicity in evaporation, and sufficiently high dielectric constant (LBL and DM). The thin-film structure (LBL/DM) employed at the start of this program was composed of a SiO_x/Sn cermet structure, followed by the $\text{ZnS}/\text{NaAlF}_4$ dielectric mirror. This structure suffered from: (1) partial decomposition due to interaction between the mirror and the overlaid liquid crystal; and (2) an inability to withstand the high temperature (450°C) required for proper substrate annealing following the thin-film deposition. The first effort was directed at replacing the dielectric mirror, $\text{ZnS}/\text{NaAlF}_4$. We found that Si/SiO_2 is an efficient replacement structure. Although Si/SiO_2 offers a considerably larger refractive index difference (3.8:1.5), it does suffer from high sheet conductivity in the silicon layers. To overcome this, we experimented with various temperatures and rates of the silicon deposition and have succeeded in obtaining the required sheet resistivity of above $10^{12} \Omega/\square$. Experimentation with the SiO_x/Sn cermet was combined with the new Si/SiO_2 DM; the annealing of this structure sharply improved the performance of the light valve (more than a fourfold increase in the switching ratio).

C. SCALE UP TO 2 IN.

This task required that we:

- Design and fabricate a complete 2 in. assembly, including glass electrode holders, electrical connection, mechanical mounting, etc.
- Design and fabricate a complete set of photomasks for the Si processing step.
- Experiment with slicing, thinning-down, and polishing of the 2 in. diameter, 5-mil-thick Si wafers.

- Implement the guard-ring solution (3rd electrode) to solve edge-breakdown,*), both on the 2 in. Si wafer and in the light-valve assembly.
- Up-grade the optical testing bench to have a 2 in. clear aperture both in the imaging and the projection optics.

All of these tasks were successfully carried out.

The assembly design relied basically on the 2 in. CdS LV assembly. Some modifications were made to permit the introduction of the third electrode into the cell. The substrate electrode, a 1/4-in.-thick, 2.25-in.-diameter fiber optic plate, was coated with a continuous layer of indium tin oxide (ITO). This was followed by evaporation of a 1.7-in.-diameter, 4- μ m-thick, and 0.1-in.-wide In ring acting as a conductive support to the substrate. The counter-electrode was also coated with 400 Å of ITO, followed by a liquid-crystal alignment layer. The conductive layer was patterned to fit the active area of the device (1.7-in. diameter). A liquid-crystal spacer ring (discontinuous) consisting of 12 to 16 μ m SiO_x was evaporated on the counter-electrode. The cell holders consist of two anodized aluminum pieces with an O-ring fitting to enable sealing of the cell. The various parts of the holder assembly are shown in Figure 13.

The photomask set design was aimed at yielding both types of edge protection (macro-channel-stop and dc-biased guard ring) as well as peripheral test devices (outside the active area). It consisted of:

- A macro-channel stop mask for boron diffusion at the periphery of the active area.
- A micro-grid pattern at the active area. Two patterns of 33 μ m (30 lines/mm) and 20- μ m (50 lines/mm) periodicity of the main light valve and the test devices.
- An oxide etch/guard-ring implantation mask to enable the guard-ring diode implantation.
- A guard-ring contact metalization mask.
- A back-contact metalization mask.

*This effort is described in detail in the following subsection.

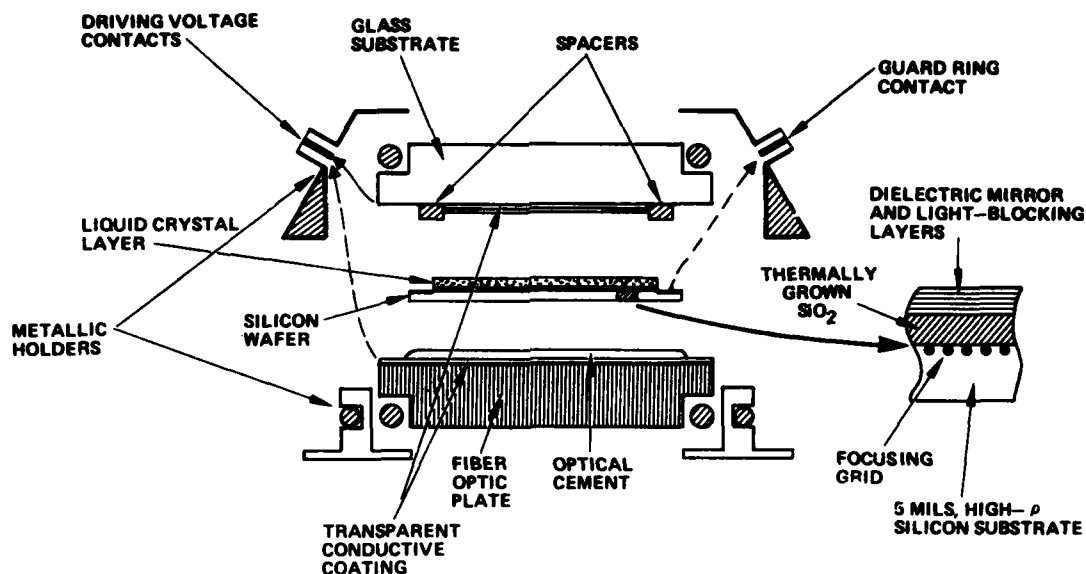


Figure 13. The silicon liquid crystal light-valve assembly.

Two types of photomask coating (emulsion and chrome) in two polarities were produced. The photomasks were fabricated by the Hughes Ground Systems Group (GSG) facility in Fullerton.

D. SOLUTION TO THE EDGE-BREAKDOWN PROBLEM

This phenomenon, appearing as an image saturation as the depletion voltage increases toward the required level, has resulted in both poor image uniformity and a substantial loss of resolution. In parallel to the present contract effort this problem was attacked under our own IR&D program.

The edge-breakdown effect is believed to be caused by the injection of minority carriers (electrons) into the active area from the edges and thus results in the collapse of the depletion region and the creation of an inversion layer at the Si/SiO_2 interface. The conclusion that minority carrier injection is causing this effect is based on three facts. First,

such edge-injection effects have been observed in MOS devices at the electrode-edge regions, and minority carrier injection was then believed to be the cause.³ Second, an increase in the depletion voltage enhances the edge-breakdown. This increase in depletion voltage widens the depletion region, thereby causing a greater generation of minority carriers, which enhances the build-up of the minority-carrier inversion layer. Third, in the photoactivated device, the edge effect is usually enhanced by increasing the writing light intensity. This points again to the conclusion that minority carrier injection enhanced by photo-generated carriers is responsible for this effect.

Former studies revealed that: (1) edge-breakdown can be reduced by constructing the counter electrode (CE) so as to remove the electric field from the Si/p^+ interface (recessed structure); (2) edge-breakdown can also be reduced by maintaining a larger spacing between the CE and the MOS structure; and (3) in addition to edge-breakdown, central-breakdown or local image saturation regions sometimes occur. These regions behave in response to changes in depletion voltage and light level, much as edge-saturated regions do. These observations suggested several possibilities as to the cause of edge-injection: (1) diffusion of carriers from the undepleted region adjacent to the edge; (2) minority carriers generated by lateral electric field breakdown; and (3) enhanced surface generation in laterally depleted regions. For the first possibility, carriers from within a region of approximately one diffusion length ($\sqrt{D\tau}$) reach the active-area edge into which they are swept by the electric field and thereby form an inversion layer at the edge. Because of the focusing effect of the electric field, resolution cells located within the active area do not "see" minority carriers generated in neighboring cells; however, those located at the edge do receive contributions from peripheral non-depleted regions. Assuming a generation lifetime of 10 μsec , and taking $D \approx 30 \text{ cm}^2/\text{sec}$ (both for depleted and nondepleted regions), the ratio of minority-carrier generation in an edge resolution element to that in a central element is approximately 60. This shows that very high minority carrier density is expected at the edge.

The second possibility is the generation of minority carriers by the breakdown of the lateral electric field. The abrupt termination of the voltage at the electrode edge may cause avalanche multiplication if the resultant field exceeds $\sim 10^6$ V/cm. For 20 V applied to the electrode, the lateral spread of the transition region under the electrode edge required to produce breakdown should be about 200 Å. Although such a narrow transition region is not expected, localized defects may produce breakdown at lower fields.

The third possibility, enhanced surface generation in the lateral depletion regions,^{3,8} relies on the fact that surface generation is limited by the creation of the inversion layer. This means that this generation component, which normally loses its significance after formation of the inversion layer in the region under the gate electrode, will still be significant in regions depleted laterally beyond the counter-electrode projection since no inversion layer will be formed there. (Lateral depletion is expected to extend roughly to the same depth as in the bulk.) The possible approaches were to:

- Use a laterally graded field electrode. This should provide a solution if the second mechanism (lateral field induced injection) is responsible for this effect.
- Use a specially designed recessed electrode to minimize the lateral distance to the edge-protection p^+ layer (~ 0.5 mil). This would solve the problem if either diffusion injection or unlimited surface generation is the mechanism responsible for this effect.
- Use a dc-biased diode guard ring. This, regardless of the possible injection mechanism (1, 2, or 3), should provide an infinite sink for the minority carriers injected from the edge. The penalty is the more complex device processing to include the diode ring, and the addition of a third electrode and the associated dc power supply.

We have not attempted the first approach since it is difficult to implement and would provide a solution for only one possible mechanism. We have experimented extensively with the second approach by: (1) varying the distance from the p^+ ring to the recessed electrode; and (2) by providing a graded field at the unavoidable passage of the electrode across the

p^+-n region. Although both modifications seemed to help, the yield of devices free of edge-breakdown was still too low. The use of a higher-resistivity silicon material turned out to be impractical since the excess doping introduced during the various processing steps was the major factor determining the ultimate doping level. Thus, processing would negate the initially higher resistivity (lower doping level). We therefore turned to the last approach, the dc-biased diode guard ring. A new set of photo masks was accordingly designed and fabricated. The guard-ring implementation in the Si processing consisted of cutting a ring 1.7 in. in diameter and 20 mils wide into the gate oxide, implanting the underlying n -silicon with phosphor, and then evaporating a contact metal on top of the implanted area. We had to experiment with the dosage and energy of implantation. Since the depth of the diode is largely determined by the drive-in temperature cycle, the optimized energy was set quite low (150 KeV). The results of optimizing the implanted dosage yielded $\sim 1.10^{13}$ A/cm². A severe problem encountered was the high leakage of this ring diode — in excess of 20 mA for a ring area of ~ 0.5 cm². The migration or spiking of the contact aluminum was suspected. To deal with the problem, we (1) lowered the thin-film anneal (which is done following Al-contact evaporation) from 500°C to 425°C and (2) introduced an intermediate polysilicon layer sandwiched between two Al contact layers. This reduced the leakage current to an acceptable level of about 1 mA. After modifications, the implementation of the dc-biased ring (biased at 40 to 50 V positive with respect to the substrate) was very successful. Edge breakdown was completely eliminated, and depletion voltage could be increased to the desired level of 30 to 40 V.

E. ACHIEVEMENT OF THE DESIGN GOALS FOR SWITCHING RATIO, RESOLUTION, AND TIME RESPONSE

The improved thin-film structure detailed above enabled implementing the annealing process. Annealing is required after thin-film deposition and (1) reduces the damage caused by X-ray radiation generated by the E-beam and (2) relieves the stress on the substrate caused by thermal mismatch during thin-film deposition. The results of the thin-film anneal were quite impressive: the switching ratio (signal-to-noise ratio) jumped from 2:1 up to 10:1, due 35

predominately to the reduction in the dark current following annealing. The switching ratio is a key factor in achieving the high-performance multimode operation discussed earlier. The achievement of up to a 10:1 switching ratio demonstrated conclusively the advantage in the use of the silicon photoconductor for the multimode application. The implementation of the 50 line/mm (20 μ m cell size) microdiode grid, as explained earlier, coupled with the successful solution of the edge-breakdown problem, allowed 44 lines/mm.

The reduction in the thickness of the thin-film by eliminating the LBLs allowed the liquid-crystal-limited 20 msec response time to be realized. Response time is another major parameter in which the silicon supersedes the CdS light valve. In the latter, the response time is limited by the detrapping time of the CdS photoconductor rather than by the liquid crystal. Figures 14 and 15 display the spatial frequency transfer curve and the linearity. Figure 16 shows the improvement made in the time response. Table 1 sums up the current performance of the 2-in. light valves.

As can be seen, most of the expectations in terms of the performance of the Si light valve — particularly with respect to speed, contrast, multimode operation (color range and b/w gray scale), switching ratio, and linearity — were realized during this program.

F. THE MULTIMODE THEORETICAL PROGRAM

1. Tasks

The present multimode theoretical program was aimed at developing a computer program to numerically calculate the characteristic transmission curves of the liquid crystal light valve (LCLV) under an electric field using the hybrid field effect (HFE) mode of operation. The goals of the program were to:

- Study theoretically the electro-optic effects in the twisted nematic liquid crystal cell
- Evaluate numerically the characteristic curves of the LCLV under the HFE mode of operation
- Evaluate the effects of the cell thickness, twist angle, and polarization of the impinging light
- Optimize the LCLV parameters for multimode operation.

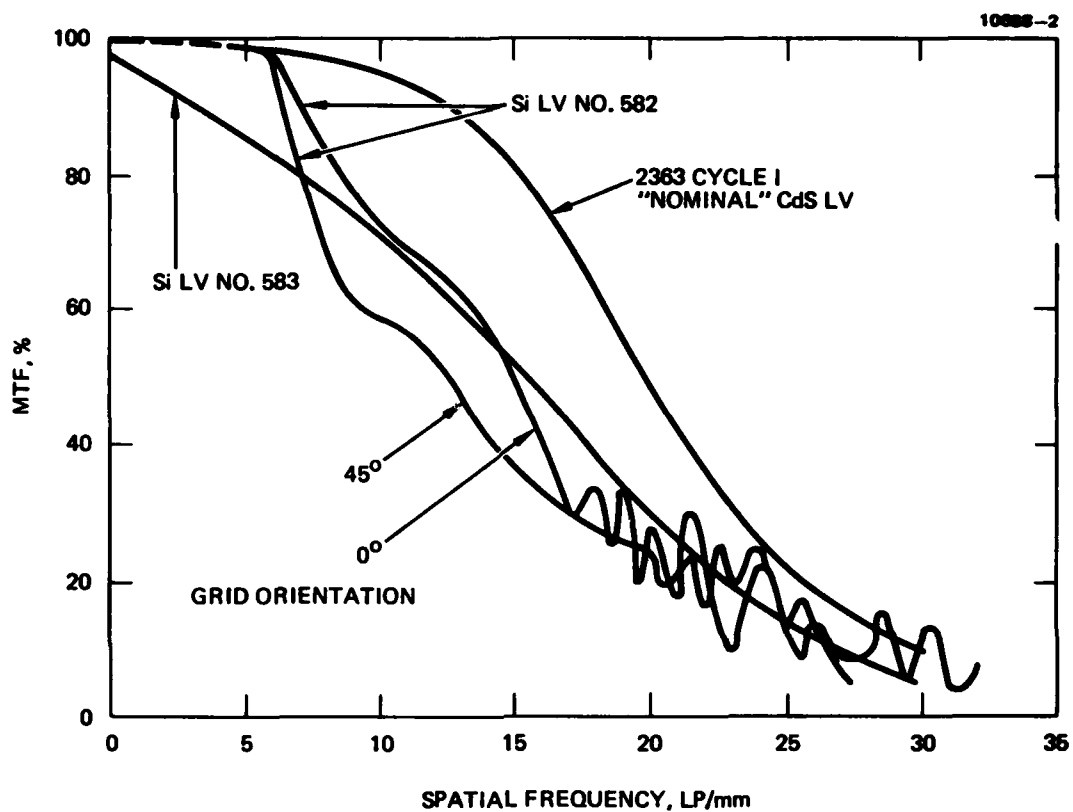


Figure 14. Comparison of good CdS and 50 L/mm silicon light valve MTF characteristics.

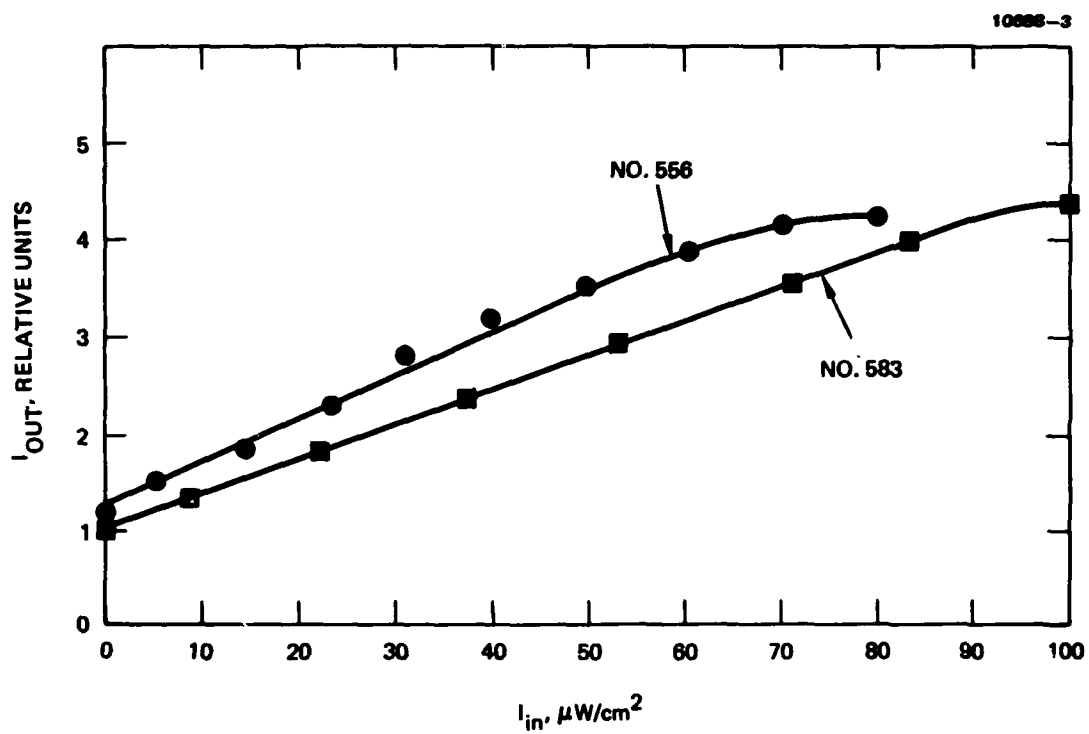


Figure 15. The silicon liquid crystal light valve response curve.

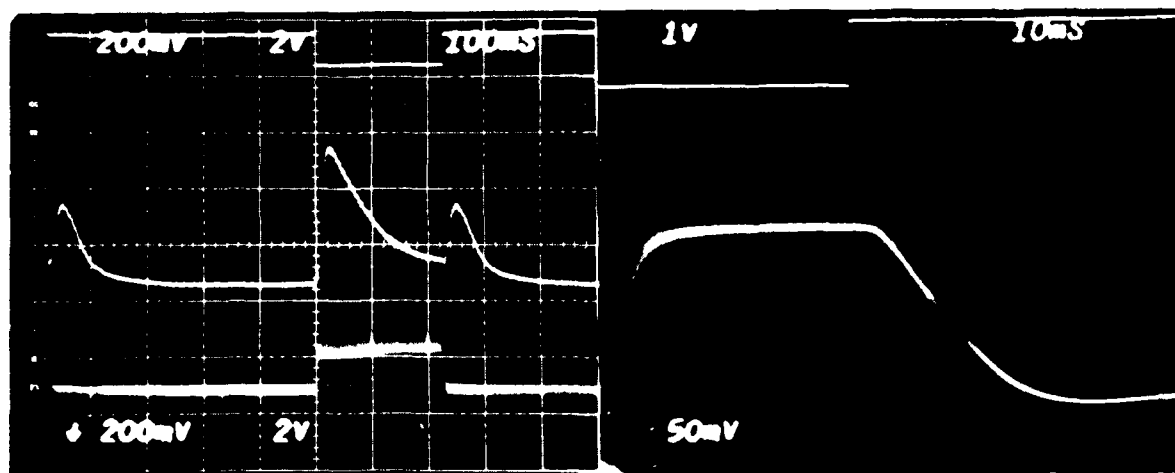


Figure 16. LV response to input photopulse.

Table 1. The Silicon Liquid Crystal Light Valve Current Performance

10000-4

- RESOLUTION - 25 LP/mm LIMITING (16 LP/mm AT 50 % MTF)
LIMITED BY PRESENT GRID (20 μ m PERIODICITY)
- SENSITIVITY UP TO 20 μ W/cm²
- CONTRAST RATIO 30:1 (LC ALIGNMENT - LIMITING FACTOR)
- RISE/DECAY TIMES 10/40 ms (LC - LIMITED)
- MULTIMODE OPERATION: 3 COLORS + FULL GREY SCALE
- NONLINEAR RESPONSE: LESS THAN 10 % IN 80 % OF
OPERATIONAL REGION
- VERY GOOD REAL-TIME TV PROJECTION (LAG FREE OPERATION)

In general, all four goals were accomplished, which led to the fabrication of deliverable multimode light valves with either cadmium sulfide or silicon photosensors. Moreover, the theoretical insight gained into the complex electro-optic effects of the LCLV under the HFE mode of operation produced other benefits relevant to the general progress of the light-valve program.

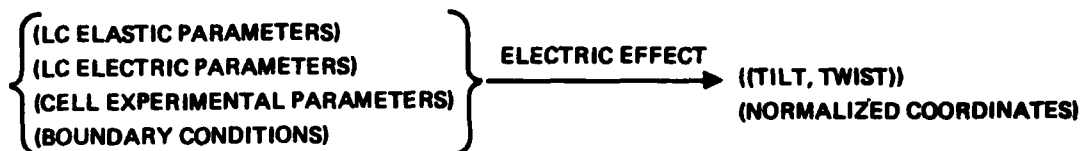
Multimode operation in which one light valve serves to produce at least three distinguishable colors for symbolic graphic display, together with a black and white TV option, has provided a challenging theoretical problem for several reasons. The HFE mode of operation is based on a combination of two fundamental optical effects: birefringence and optical activity. These effects together determine the final amplitude and phase of the light emerging from the LCLV. Moreover, the distorted configuration of the twisted nematic LC molecular arrangement under an electric field is complex and requires numerical methods for calculating the twist and tilt angles along the cell through which the light is transmitted. The experimental observation that device performance is sensitive to small variations in the three major parameters, namely, the cell thickness, the twist angle, and the polarization entrance angle, precludes making crude estimates of the required parameters for multimode operation. Thus, an in-depth understanding of the characteristics of the electro-optic device was needed; this was provided under the theoretical tasks. The theoretical model has provided the general ability to tailor the device to a specific application, to optimize its critical parameters, and to evaluate its performance under the choice of parameters and fabrication tolerances.

2. Outline of Theoretical Program

The theoretical calculation of the electro-optic transmission characteristics of the twisted nematic LC cell under the NAVSEA contract was divided into two parts (see Figure 17). In the first computer program (TILST), we numerically calculated the electric portion of the effect (i.e., the distortion of the LC twisted prealignment under the applied electric field). The second computer program is devoted to the optic effect; we numerically computed the modulation of a monochromatic polarized light through the previously

● COMPUTER PROGRAM NO. 1: "TILST"

DISTORTION OF THE LC UNDER ELECTRIC FIELD



● COMPUTER PROGRAM NO. 2: "HYBRIDEO"

TRANSMISSION OF LIGHT THROUGH DEFORMED LC LAYER

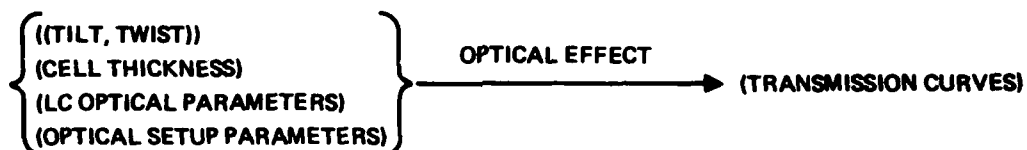


Figure 17. Diagram of the general computer approach for solving the electro-optic characteristics of the twisted nematic liquid crystal cell.

calculated deformed configuration of the LC, thus predicting the characteristic curves for the three primary colors (blue, green, red). The display performance can be evaluated from the calculated characteristic curves. The polarization entrance angle is introduced in the second program. The final electro-optic numerical results were correlated with experimental characteristic transmission curves for several LC cell configurations, thus testing the validity of the approximations involved in the numerical methods. Finally, we calculated the transmission characteristic curves for the multimode cells that were delivered under the present program.

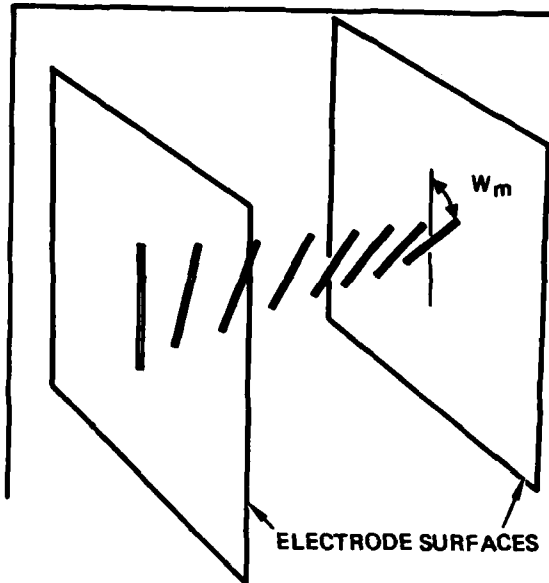
3. The Electric Effect

A numerical method was developed for calculating the distorted LC molecular configuration in the twisted nematic LC cell under an applied electric field. The mathematical boundary conditions of the problem are determined

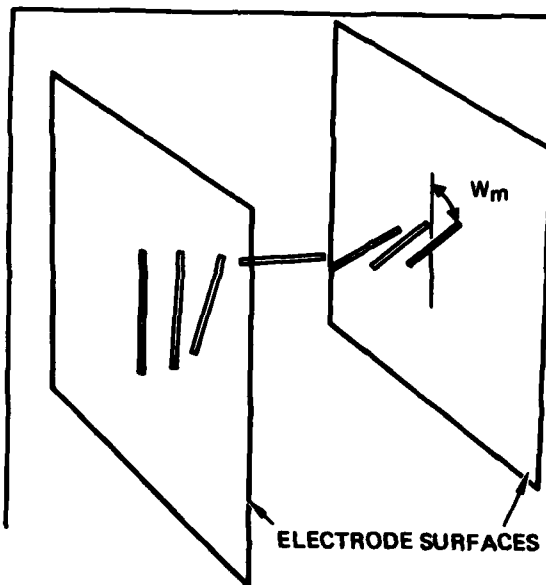
from the architecture of the cell. The twisted nematic cell is made by filling the spacing between two transparent conducting electrodes with positive dielectric LC ($\epsilon_{\parallel} > \epsilon_{\perp}$). Homogeneous (parallel) alignment near each of the electrodes is maintained through parallel anchoring of the LC molecules. This is practically achieved by specially treating the surfaces. The alignment of the two electrodes is rotated with respect to each by a twist angle, W ; therefore, in the off-state (no voltage), the parallel LC molecules will twist gradually in a screw-like pattern (see Figure 18(a)). When an electric field above a certain threshold ($U > U_{th}$) is applied on the electrodes, the molecules that are less tightly anchored will tend to realign parallel to the applied field, namely, toward a perpendicular direction to the electrodes, thus maintaining new tilt (ϕ) and twist (W) angles in the equilibrium state (see Figure 18(b)). Due to the birefringence properties of the LC molecules, this realignment will modulate polarized light which is transmitted through the layer.

The equilibrium model is based on the continuum description of the LC as developed by Oseen⁴ and Frank.⁵ After the electric field is applied, the LC twisted system will obtain a new state of equilibrium which satisfies the thermodynamic minimization of the free energy.^{6,7} Maxwell's equation accounts for the dielectric properties, and the integral limits are determined by the boundary conditions. The numerical method⁸ (Figure 19) starts with the basic elastic and dielectric parameters of the LC and the experimental cell parameters (maximum twist angle, W_m , and the reduced voltage, U/U_0) and calculates, through an optimization routine, the maximum tilt angle, ϕ_m , and the integration parameter, β . Then an integration routine calculates the tilt angle, ϕ , and twist angle, W , along the reduced cell's length, (Z/L) , where L is the cell thickness. An Amdel 470 computer was used with the IMSL subroutine, ZXSSQ, which allows the convergence algorithm^{9a,b} to be achieved in less than 10 iterations, with accuracy close to the limit of the computer noise.

Utilizing the above-mentioned portion of the TILST program to calculate the values of ϕ_{max} and β , the second part of the TILST computer program was run to obtain the tilt and twist angles of the LC molecules along the twisted nematic cell. The results for the tilt and twist angles for different cases were tabulated and stored in the computer disk. An example of 42



(a) NO VOLTAGE



(b) INTERMEDIATE VOLTAGE

Figure 18.
 Perspective look at the twisted
 nematic liquid crystal prealignment
 with maximum twist, W_m , used in
 the hybrid field mode of operation.
 (a) No voltage (off state).
 (b) Intermediate voltage (on
 state).

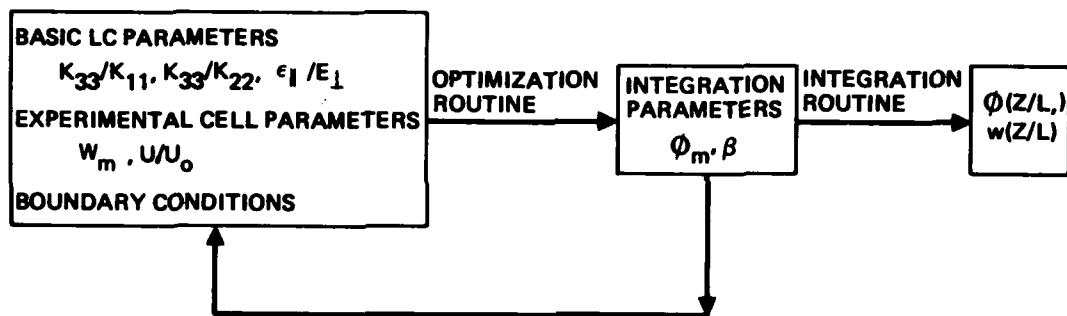


Figure 19. Flow chart of the TILST computer program.

the results is shown in Figure 20. The LC parameters are those of the E7 LC mixture (Table 2) used in fabricating the LCLV at Hughes Aircraft Co. The results were carried out for a wide spectrum of maximum twist angles ($0^\circ < W_m < 90^\circ$, cell thickness, $2 \mu\text{m} < L < 16 \mu\text{m}$, polarized entrance angle, $0^\circ < \alpha < W_m/2$, and reduced voltages, $0 < U/U_0 < 6$) which are currently used in the LCLV operation.

As expected, the electric field first tilts the molecules at the center of the cell, far away from the surface anchoring forces; as a consequence, the twist spiral begins to breakdown (Figure 20). At intermediate voltage, the twist angle can be separated into three regimes. Near each electrode, the tendency is greater for the LC molecules to adopt the almost parallel alignment imposed by the electrode's surface treatment. The molecules in the central portion of the cell transfer the twist. The molecules in this region are highly tilted (Figure 20(a)) and approach the perpendicular orientation asymptotically as the voltage is increased. Thus, the central region contributes only minimally to the birefringence effect; the major effect will be due to the outside portions near the electrodes. At higher applied voltages, the central high tilt region extends practically along the entire cell, thus providing an almost optical isotropic medium to light impinging normal to the electrodes.

A more detailed computer calculation of the distorted configurations of the LC molecules along half of the twisted nematic LC cells are shown in Figures 21 and 22 for a maximum twist angle of $W_m = 45^\circ$ and applied electric fields in the range $1 < U/U_0 < 5.5$. Since, as in Figure 20, symmetry considerations apply, only the data for half of the cell is presented in Figure 21 for the tilt angle, and in Figure 22 for the twist angle. The basic parameters for the E7 liquid crystal were taken from Table 2.

4. The Optical Effect

A computer program needs to be developed to calculate the transmission characteristic curves. The most common operating condition of the hybrid field mode assumes that the angle between the polarization vector of the incident light and the detector of the LC molecules at the front surface is 0 (or $i = 90^\circ$). However, in some applications other incident angles have certain advantages, as discussed below, with respect to the multimode operation. Due

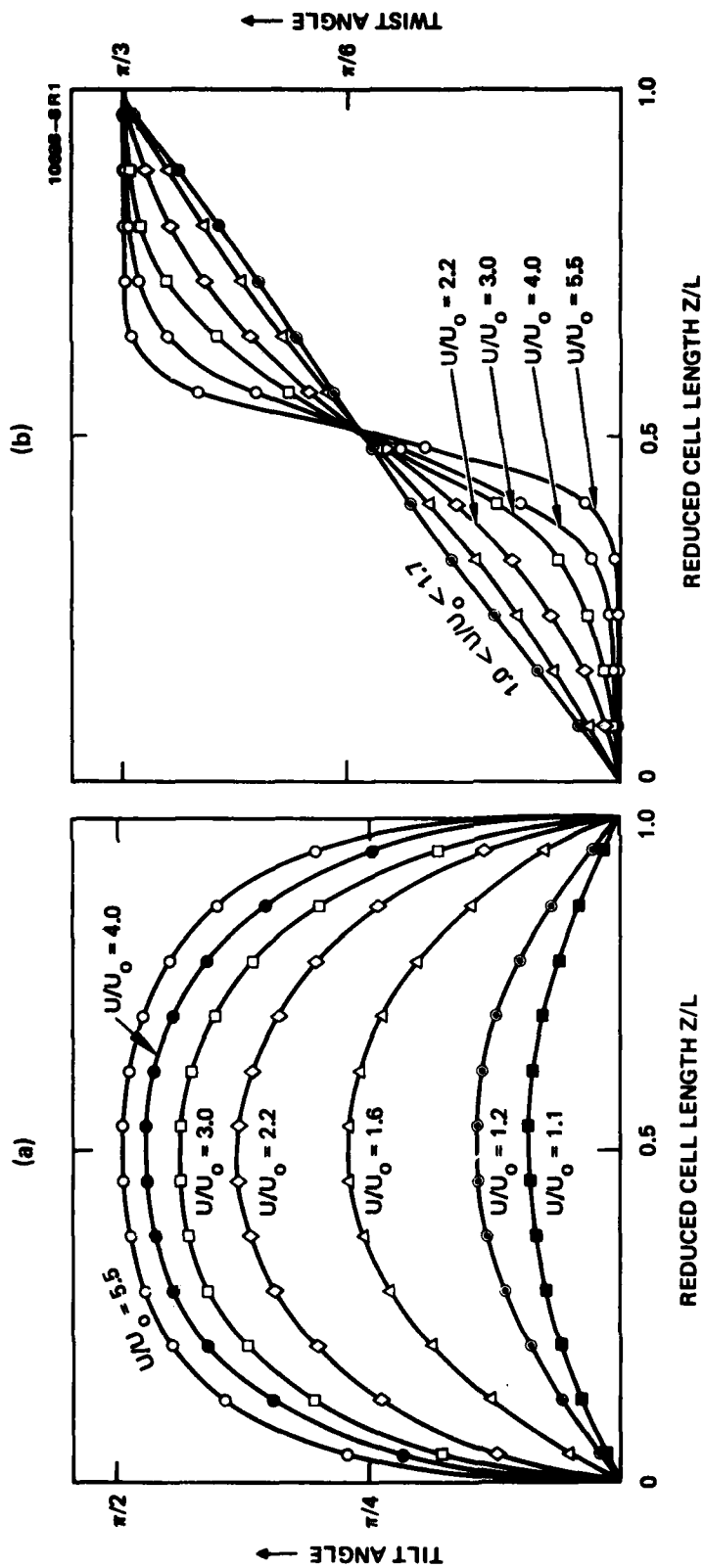


Figure 20. The (a) tilt angle and (b) twist angle along the twisted nematic LC cell as computed by the TILST computer program for maximum twist angle 60° and E-7 type LC mixture - $1 < U/U_0 < 5.5$.

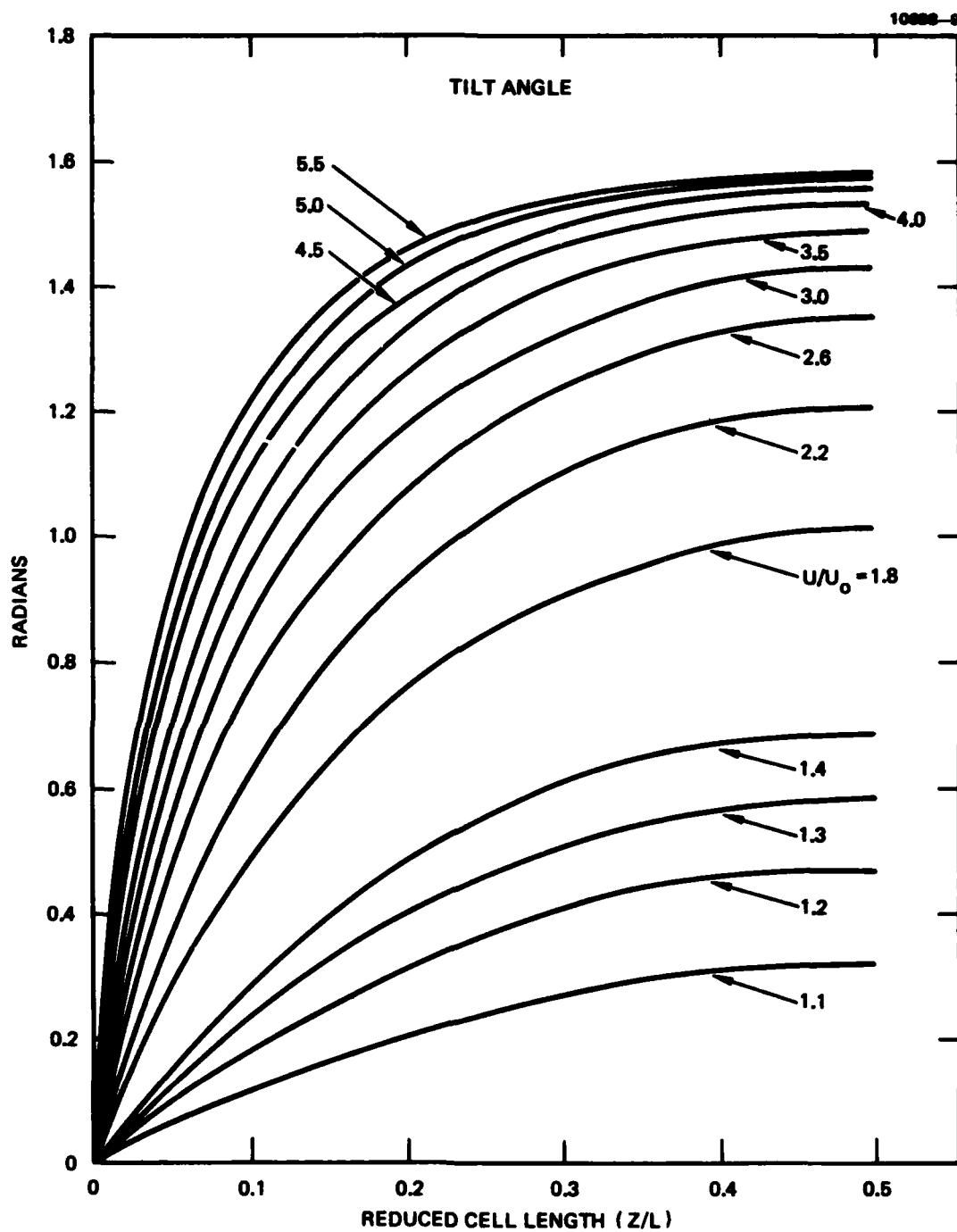


Figure 21. Theoretical calculation of the tilt angle along the twisted nematic LC cell for $W_m = 45^\circ$ and $1 \leq U/U_0 \leq 5.5$.

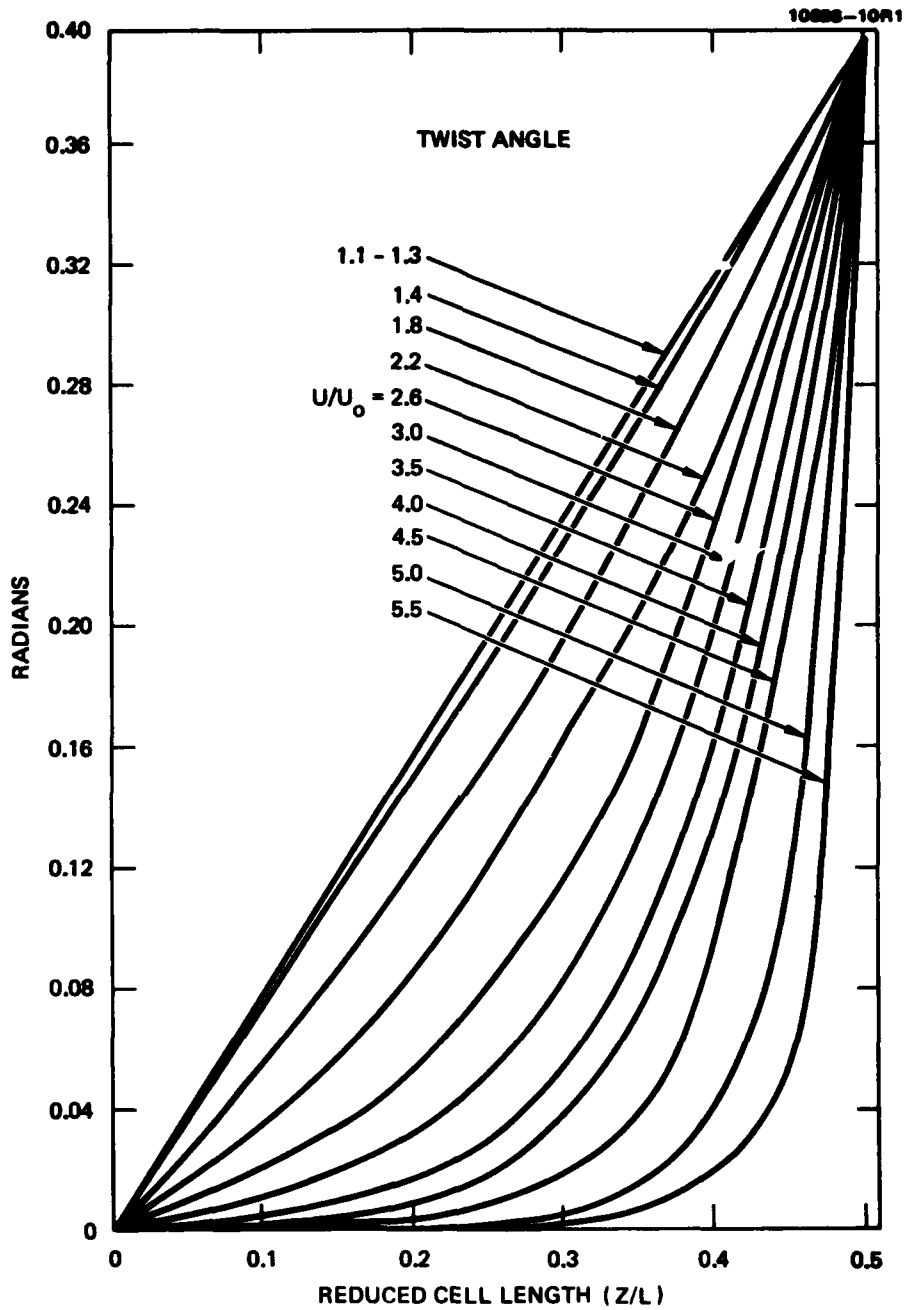


Figure 22. Theoretical calculation of the twist angle along the twisted nematic LC cell for $W_m = 45^\circ$ and $1 < U/U_0 < 5.5$.

Table 2. Basic Parameters of the
E7 LC Mixture

$$k_{11} = 9.5 \times 10^{-12} \text{ MKS}$$

$$k_{22} = 8 \times 10^{-12} \text{ MKS}$$

$$k_{33} = 18 \times 10^{-12} \text{ MKS}$$

$$\epsilon_{\parallel} = 16$$

$$\epsilon_{\perp} = 5$$

$$\kappa = 0.89$$

$$\alpha = 1.25$$

$$\gamma = 2.2$$

$$U_0 = 0.98 \text{ V}$$

to the inert helical alignment of the LC molecules, in the case where the electric field is less than the threshold applied to the cell (off-state; i.e., absence of writing information), the optical activity effect will tend to rotate the polarization of the light to follow the twisted configuration of the LC molecules. On reflection from the DM (dielectric mirror) the light will pass a second time through the LC layer where its polarization will be rotated back (Figure 23(a)). For the proper choice of cell thickness,¹⁰ the readout light emerging from the LCLV can be blocked by an analyzer oriented to pass only light polarized perpendicular to the initial polarizer. However, for cells with high twist gradient, some residual birefringence effect can cause the emerging light to become elliptically polarized, and the off state will not provide a completely blocked condition for certain wavelengths.

In the on-state, when an electric field is applied on the LC layer above a certain threshold voltage (optical information in the read-in channel activates the photosensor layer), the positively anisotropic LC molecules will tend to realign perpendicular to the electrodes. In general, the electric field will first tilt the molecules at the center of the cell where the surface anchoring forces are the weakest (Figure 18(b)), thus partially destroying the twist spiral. As explained above, at intermediate voltages the twist angle distribution can be separated into three regimes. Near each electrode a large portion of the LC molecules will tend to adopt almost parallel alignment as imposed by the surface anchoring forces; however, a partial spiral is still maintained. The center regime of the cell, which consists of highly tilted molecules, separates these two almost parallel regimes. An ideal birefringent configuration for the hybrid field mode of operation will mean neglecting all of the residual spiral twist in the outside regimes, thus providing two parallel molecular alignment regions, with angle W_m in between, separated by a completely perpendicular molecular alignment regime at the center of the cell. The polarization of the light going through a completely perpendicular LC alignment at the center will be unaffected. The linear polarized light along the front parallel LC molecules will become elliptically polarized from the rear regime of birefringent molecules. On reflection from the DM, the cumulative birefringent effect will cause the emerging light to become elliptically polarized, thus allowing transmission

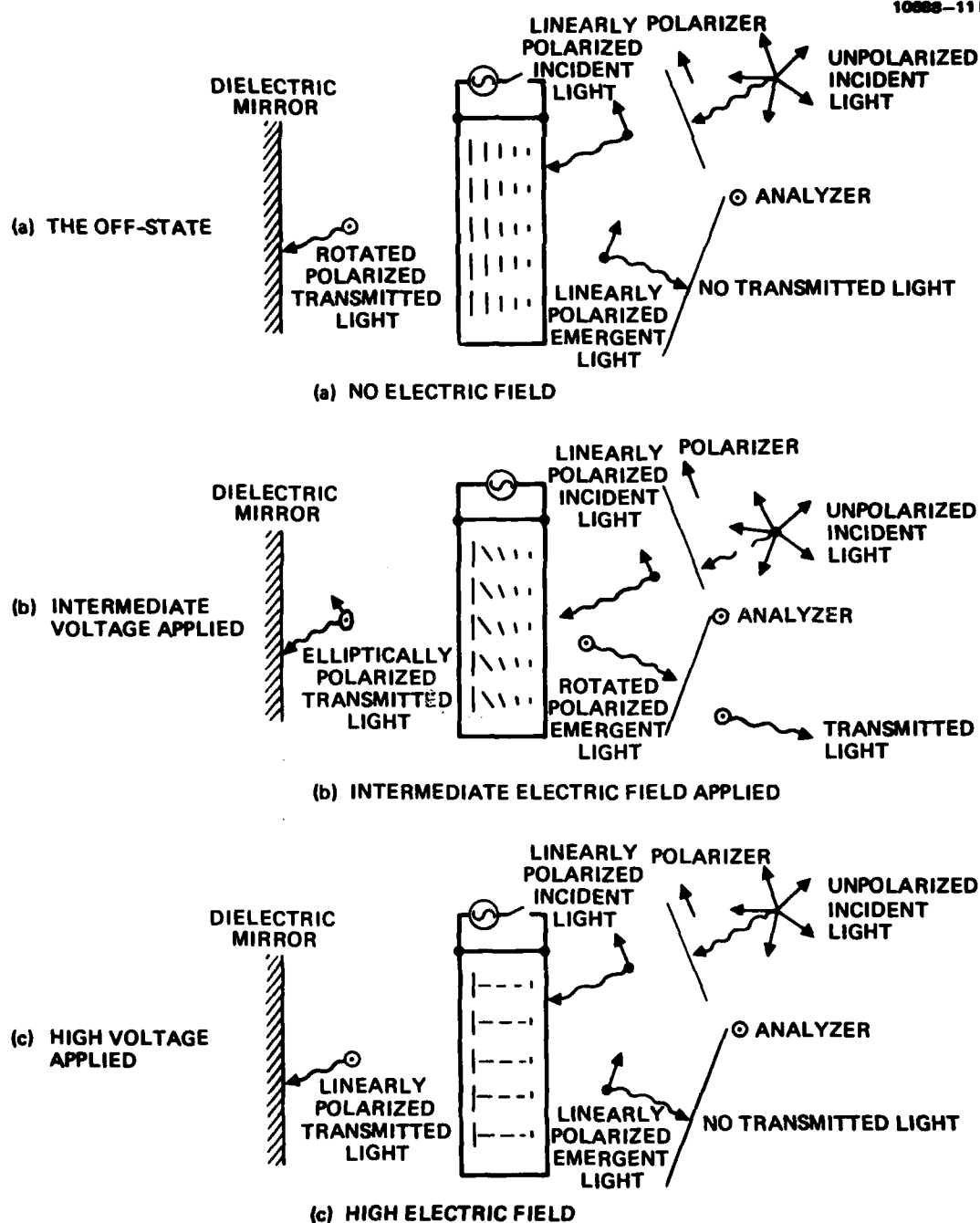


Figure 23. A schematic representation of the operation of the hybrid field effect mode in (a) the off state; (b) with intermediate voltage applied; (c) high voltage applied.

through the crossed analyzer (see Figure 22(b)). At still higher voltages, the perpendicular tilt regime starts to dominate through most of the cell, and another state of dark output is expected through the crossed analyzer (Figure 23(c)).

In non-ideal situations, as demonstrated, for example, in Figure 20, the deformed configuration of the LC molecules under the influence of an electric field will allow both the optical activity effect, due to partial spiral arrangement, and the birefringence effect of the anisotropic LC molecules to play a role in the final state of polarization of the emerging light from the LCLV. A successive calculation of the optical effect which follows the changes in the light polarization along the deformed LC molecular arrangement will enable us to evaluate the modulation of the light emerging from the LCLV device for different electric fields.

The transmission of polarized light through the anisotropic medium of the twisted nematic cell is rather complicated because both the optical activity and the birefringence effect play a role. This suggests a numerical solution in which the cell is dissected into a series of thin layers. For each layer a simplified molecular configuration is assumed, allowing a successive calculation of the optical effects. The building block of the numerical routine in the present computer program (HYBRIDEO)¹¹ reduces to the calculation of the transmission of polarized light through a constant twist-rate nematic-anisotropic layer. This problem can be solved analytically by using the coupled mode theory.¹² For slow twist rates, using the weak coupling approximation and neglecting the reflected waves lead to simple analytic expressions for the Maxwell equations describing the coupled system. We dissect the LC cell into n cells and assume each layer to have a constant gradient for the twist angle and a constant averaged tilt angle. The flow chart of the HYBRIDEO program (Figure 24) shows the successive calculation of the transmission of the polarized light through the dissected cell. The tabulated data calculated in the previous TILST program for the deformed configuration of the LC molecules along the twisted nematic cell serve as an input for the optical calculation. The experimental setup of the polarizer for the incoming beam and the analyzer for the outgoing beam are set, and characteristic transmission curves are calculated for three primary colors: blue (466 nm), green (545 nm), and red (623 nm). An example of the

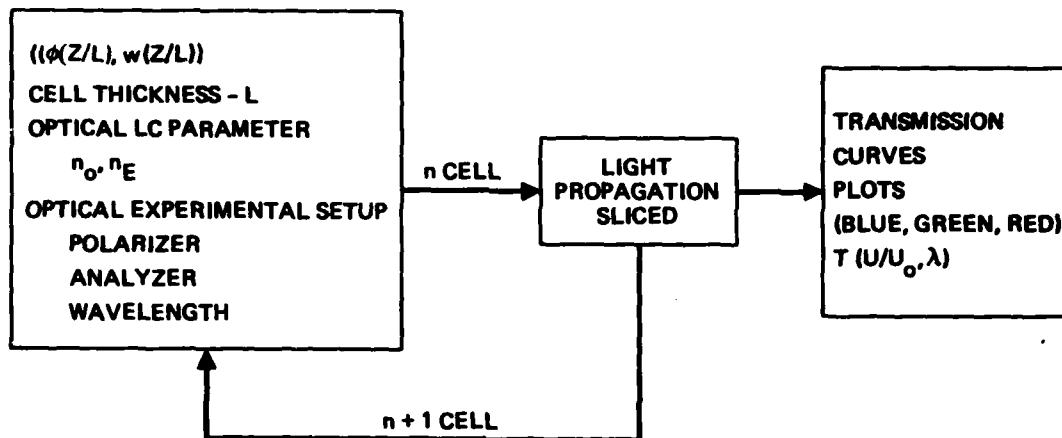


Figure 24. Flow chart of the HYBRIDEO computer program.

calculated transmission curves for a $16 \mu\text{m}$ cell and $W_m = 60^\circ$ using polarized light parallel to the LC detector at the front surface ($i = 0^\circ$) are shown in Figure 25. The experimental transmission curves for a twisted nematic cell with the same parameters using 100 \AA bandwidth monochrome filters at the specified wavelengths and a 5° cone input condensing lens are shown in Figure 26. The experimental data¹¹ was taken for the LCLV H17604-21-D light valve,, which was fabricated and measured under NAVSEA contract N00024-76-C-5366 and delivered to the Navy in late 1976. A comparison of the shapes of the theoretical and the experimental curves indicates a good agreement, thus assuring the validity of the approximations on which the computer programs are based.

G. MULTIMODE OPTIMIZATION AND BACK SLOPE MODE

1. Results

Under the present task, we numerically calculated the characteristic transmission curves of over 150 cases, chosen from among those cell configurations having potential use for LCLV fabrication. The following parameters were considered: cell thickness ($2 \mu\text{m} < d < 16 \mu\text{m}$), maximum twist angle ($0 < W_m < 90^\circ$), and polarization angle (with respect to the LC detector at the front surface of the device ($0 < i < W_m/2$)). From the study of the variety of characteristic curves we concluded that to meet the multimode goal of simultaneous operation of three color symbolic graphic and black white gray scale TV, while at the same time taking into account the constraints of the present switching ratio limitation ($S.R. < 2.5$), the back slope mode (BSM) of operation is preferable. In the BSM configuration, the polarizer is oriented at half of the maximum twist angle ($i = W_m/2$), and the analyzer is oriented 90° with respect to the polarizer. At low voltages above the threshold, birefringence and optical activity are the dominant effects. The resulting narrow-band spectrum filter separates the various colors and enables graphic display with distinguished colors. At some higher voltages, a partial compensating effect of the birefringence occurs due to the internal symmetry of the molecular arrangement of the LC molecules (Figures 21 and 22); this partial compensation results in a broad-band spectrum filter, namely, white gray-scale operation on the back slope of the characteristic curves. Finally, at some higher electric field the compensating effect will dominate, causing a total blacking (off-state) at voltages not too high to be achieved under the

through the crossed analyzer (see Figure 22(b)). At still higher voltages, the perpendicular tilt regime starts to dominate through most of the cell, and another state of dark output is expected through the crossed analyzer (Figure 23(c)).

In non-ideal situations, as demonstrated, for example, in Figure 20, the deformed configuration of the LC molecules under the influence of an electric field will allow both the optical activity effect, due to partial spiral arrangement, and the birefringence effect of the anisotropic LC molecules to play a role in the final state of polarization of the emerging light from the LCLV. A successive calculation of the optical effect which follows the changes in the light polarization along the deformed LC molecular arrangement will enable us to evaluate the modulation of the light emerging from the LCLV device for different electric fields.

The transmission of polarized light through the anisotropic medium of the twisted nematic cell is rather complicated because both the optical activity and the birefringence effect play a role. This suggests a numerical solution in which the cell is dissected into a series of thin layers. For each layer a simplified molecular configuration is assumed, allowing a successive calculation of the optical effects. The building block of the numerical routine in the present computer program (HYBRIDEO)¹¹ reduces to the calculation of the transmission of polarized light through a constant twist-rate nematic-anisotropic layer. This problem can be solved analytically by using the coupled mode theory.¹² For slow twist rates, using the weak coupling approximation and neglecting the reflected waves lead to simple analytic expressions for the Maxwell equations describing the coupled system. We dissect the LC cell into n cells and assume each layer to have a constant gradient for the twist angle and a constant averaged tilt angle. The flow chart of the HYBRIDEO program (Figure 24) shows the successive calculation of the transmission of the polarized light through the dissected cell. The tabulated data calculated in the previous TILST program for the deformed configuration of the LC molecules along the twisted nematic cell serve as an input for the optical calculation. The experimental setup of the polarizer for the incoming beam and the analyzer for the outgoing beam are set, and characteristic transmission curves are calculated for three primary colors: blue (466 nm), green (545 nm), and red (623 nm). An example of the

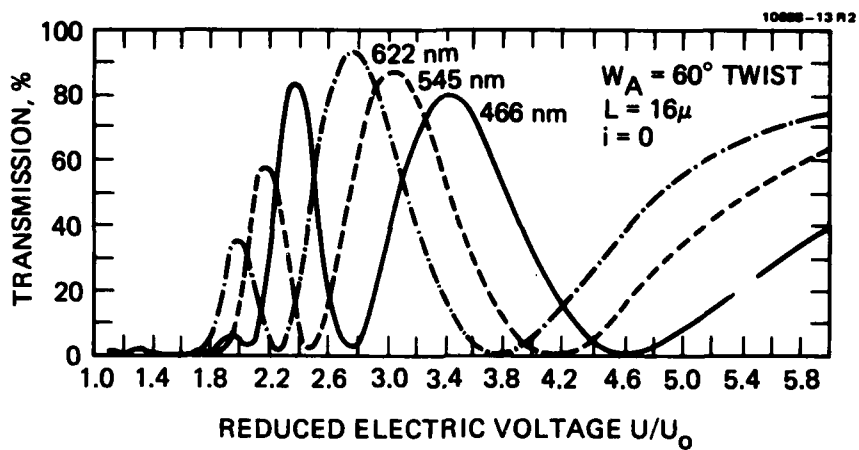


Figure 25.
Theoretical transmission characteristic curves for
 $L = 16 \mu\text{m}$ thick and $W_m = 60^\circ$ twisted nematic cell.

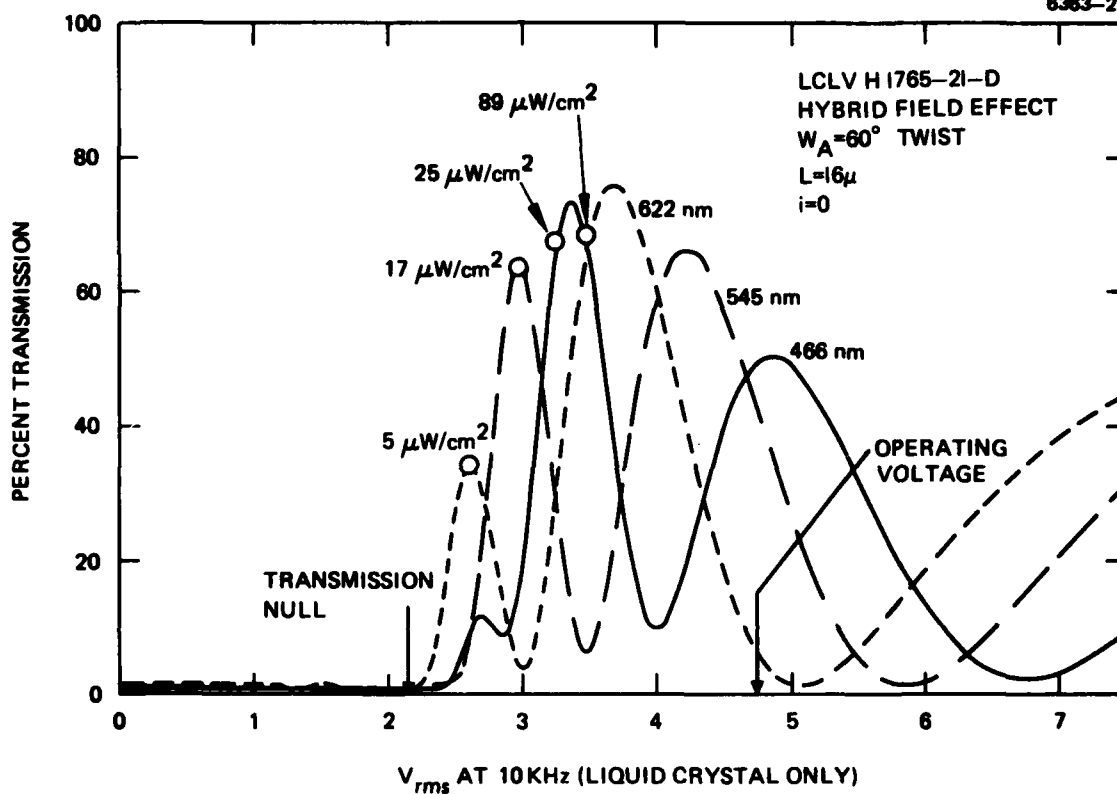


Figure 26. Experimental characteristic-transmission curves for LCLV H1765-21-D.

present switching ratio limitation of the CdS photosensor. A typical theoretical transmission characteristic curve in the BSM configuration of a 4.35- μ m-thick LCLV with maximum twist angle of 60°, input polarizer angle of 30°, and output analyzer at 120° is shown in Figure 27 for the red (623 nm), green (545 nm), and blue (466 nm) monochromatic lines. The voltages are given in normalized voltage coordinates, where U_0 is the threshold voltage, estimated at $U_0 = 0.96$ V. Multimode operation is clearly demonstrated. Under illumination by white light, the following output is theoretically expected: red at 1.2 V, green at 1.4 V, blue at 1.7 V, magenta at 2.2 V, and black and white back slope option from 2.5 V to 4.0 V. However, the present configuration was not optimized for maximum transmission output, and the final device requirement would not dictate whether to optimize the final transmission of the color symbology on account of the TV output transmission capability or vice versa.

2. Conclusions

Under the present theoretical program we developed a computer numerical method for evaluating the electro-optic effects in a twisted nematic liquid crystal cell subjected to an electric field. The numerical routines allow us to calculate the transmission characteristic curves of the LCLV under the hybrid field mode of operation. We studied the effects of the following three major parameters: cell thickness, maximum twist angle, and polarizer entrance, angle. From the general study of the theoretical characteristic curves, we concluded that the back slope operational mode is preferred for obtaining multimode mode under the present switching ratio limitations. Three multimode devices were delivered (two test cells and one CdS LCLV) which demonstrate the multimode capability of the back slope operational mode.

Beyond the mentioned tasks, the present theoretical insight into the complex electro-optic effects in the LCLV has produced other paybacks relevant to the general progress of the light valve program. We have used the computer routines for calculating the characteristic transmission curves for the monochrome graphic LCLV under the Navy N00123-77-C-0619 (Manufacturing Technology Program for Liquid Crystal Light Valve Modules) contract to improve the performance graphic display. The performance of the monochrome graphics was

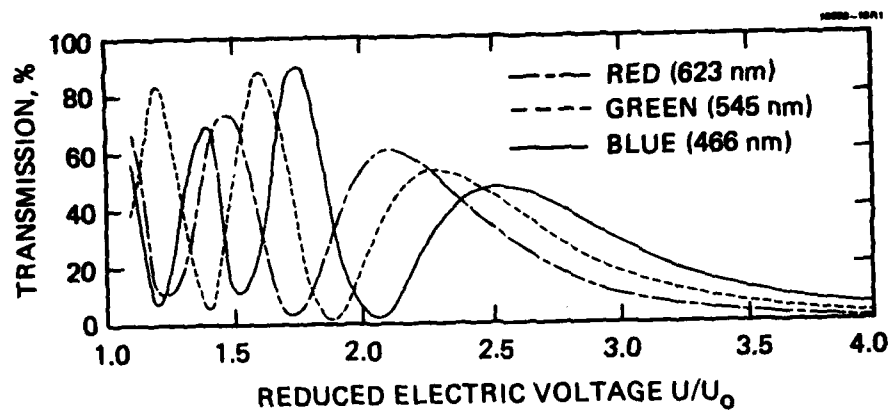


Figure 27. Theoretical transmission characteristic curves computed for the BSM configuration of a thick LCLV with maximum twist, $W = 60^\circ$, and input polarizer angle, $i = 30^\circ$.^m

evaluated for the following quality characteristics: output transmission, intensity efficiency, contrast ratio, color discrimination, display homogeneity, rise time, and decay time. The numerical routines were used to optimize the overall performance of the monochrome graphic display. Practical considerations regarding manufacturing tolerances during device fabrication, together with system requirements have lead to a theoretical evaluation of the cell parameters (thickness and maximum twist angle) to provide a better overall quality of the CdS graphics LCLV.

In general, the theoretical effort under the present program has provided a basic understanding of the device characteristics. It has enabled estimating the theoretical limit and optimization of the device performance under practical experimental constraints and system requirements. It allows estimating the fabrication tolerance requirements and tailoring the device parameters to the specific application. The theoretical effort is expected to reduce the fabrication cost.

SECTION 4

DELIVERIES

A. SILICON LIGHT VALVE DELIVERIES

1. 1 cm² Silicon Liquid Crystal Light Valve No. 386

a. General

- (1) Substrate: Silicon, HRL 8 K Ω -cm
 - MOS Structure: 850 Å thermally-grown oxide gate
 - Back Contact: Diffused Boron (p⁺) 10¹⁴/cm²
 - Macrochannel Stop: Diffused Boron (p⁺) 10¹⁴/cm²
 - Microchannel Stop: Phosphorous ion implantation 1 x 10¹²/cm²
- (2) Light Blocking Layer: Cermet-Sn/SiO_x 20 pairs
- (3) Mirror: 2 pairs of Si/SiO₂
 - Liquid Crystal Alignment: 45° angle-evaporated SiO_x
- (4) Liquid Crystal: BDH E-7 Biphenyl, Eutectic
- (5) Glass Electrodes:
 - (a) Substrate Electrode (E): 12.5 mm glass, $\lambda/4$ polished
Coating: 500 Å Indium Tin Oxide
 - (b) Counter Electrode (CE): 12.5 mm glass, $\lambda/4$ polished
Coating: 4000 Å Indium Tin Oxide; 4 μ m SiO_x-liquid
crystal spacings; 1000 Å SiO₂ - ion beam etched
for liquid crystal alignment.
- (6) Cell Construction: Anodized Aluminum Frame 1 in. x 1 in. window

b. Operating Conditions:

Voltage Waveform: Pulsed Rectangular Wave (Negative) — Frequency
1 kHz

Depletion Phase: Duration 990 μ sec; Level + 35 V

Accumulation Phase: Duration 10 μ sec; Amplitude -20 V

Note: Voltage is measured with respect to substrate electrode (E)
(i.e., counter electrode positive in depletion phase and
negative in accumulation phase with respect to substrate
electrode).

(c) Performance:

Resolution: 32 lines/mm (Air Force Resolution Target: 4¹)

Contrast Ratio: >10 at 50 $\mu\text{W}/\text{cm}^2$

Threshold Sensitivity: 10 $\mu\text{W}/\text{cm}^2$

Response Time:

Rise: 15 msec

Fall: 20 msec

2. 2 Inch Silicon Liquid Crystal Light Valve No. 680

a. General

- (1) Substrate: Silicon, Wafer 7.5 k Ω ; diameter 2 in.; thickness 0.005 in.

MOS Structure: 2500 Å thermally grown oxide gate.

Back Contact: p⁺ diffuse boron, 10¹⁴/cm².

Microchannel Grid: phosphorous ion implantation,
1 x 10¹²/cm³. 10 μ m x 10 μ m cell size.

Diode Guard Ring: phosphorous ion implantation 10¹³/cm².

Diameter: 1.7 in., Width: 0.015 in.

- (2) Light Blocking Layer/Dielectric Mirrors: 12 pairs Si/SiO₂.

- (3) Liquid Crystal Alignment: 45° angle-evaporated SiO_x.

- (4) Liquid Crystal: BDH E-7 biphenyl, eutectic, 4 μ m thickness.

- (5) Glass Electrodes:

(a) Substrate electrode: 2 in. fiber optic.
Coating: 500 Å indium-tin oxide, indium contact ring

(b) Counter electrode: 2 in. glass, $\lambda/4$ polished.

- (6) Coating: 400 Å indium-tin oxide; 4 μ m SiO_x liquid crystal spacers, 100 Å/5 Å shallow angle SiO_x deposition.

- (7) Cell Construction: Anodized Al-frame, 2 in. diameter window sealed.

b. Operating Conditions

Voltage Waveform: pulsed rectangular; frequency: 1 KHz.

Forward Slope Mode: depletion phase: +40 V, 990 μ sec.
accumulation phase: -40 V, 10 μ sec

Ring Diode Bias: +30 V, 5 mA.

c. Performance

Resolution: 50 lines/mm (4⁵ Air Force Resolution Chart)

Contrast Ratio: (at 30 μ W/cm²) 6:1.

Rise Time: 5 msec

Decay Time: 20 msec.

3. 2 Inch Silicon Liquid Crystal Light Valve No. 706

a. General

- (1) Substrate: Silicon, Wafer 7.5 k Ω ; diameter 2 in.; thickness 0.005 in.

MOS Structure: 2500 Å thermally grown oxide gate.

Back Contact: p⁺ diffuse boron, 10¹⁴/cm².

Microchannel Grid: phosphorous ion implantation,
1 x 10¹²/cm³. 10 μ m x 10 μ m cell size.

Diode Guard Ring: phosphorous ion implantation 10¹³/cm².

Diameter: 1.7 in., Width: 0.015 in.

- (2) Light Blocking Layer/Dielectric Mirrors: 12 pairs Si/SiO₂.
- (3) Liquid Crystal Alignment: 45° angle-evaporated SiO_x.
- (4) Liquid Crystal: BDH E-7 biphenyl, eutectic, 4 μ m thickness.
- (5) Glass Electrodes:
- (a) Substrate electrode: 2 in. fiber optic.
Coating: 500 Å indium-tin oxide, indium contact ring
- (b) Counter electrode: 2 in. glass, $\lambda/4$ polished.
- (6) Coating: 400 Å indium-tin oxide; 4 μ m SiO_x liquid crystal spacers, 100 Å SiO₂ ion beam etched.
- (7) Cell Construction: Anodized Al-frame, 2 in. diameter window sealed.

b. Operating Conditions

Voltage Waveform: pulsed rectangular; frequency: 1 KHz.

Forward Slope Mode: depletion phase: +40 V, 990 μ sec.
accumulation phase: -40 V, 10 μ sec

Ring Diode Bias: +50 V, 5 mA.

c. Performance

Resolution: 50 lines/mm (4⁵ Air Force Resolution Chart)

Contrast Ratio: (at 40 μ W/cm²) - 15:1

Rise Time: 10 msec

Decay Time: 26 msec.

4. 2 Inch Silicon Liquid Crystal Light Valve No. 776

a. General

- (1) Substrate: Silicon, Wafer 7.5 k Ω ; diameter 2 in.; thickness 0.005 in.
- MOS Structure: 2500 Å thermally grown oxide gate.
- Back Contact: Indium tin oxide and aluminum
- Microchannel Grid: phosphorous ion implantation, $1 \times 10^{12}/\text{cm}^3$. 10 μm x 10 μm cell size.
- Diode Guard Ring: phosphorous ion implantation $10^{13}/\text{cm}^2$.
- Diameter: 1.7 in., Width: 0.015 in.
- (2) Light Blocking Layer/Dielectric Mirrors: 14 pairs Si/SiO₂.
- (3) Liquid Crystal Alignment: 45° angle-evaporated SiO_x.
- (4) Liquid Crystal: BDH E-18 biphenyl, eutectic, 4 μm thickness.
- (5) Glass Electrodes:
- (a) Substrate electrode: 2 in. fiber optic.
Coating: 500 Å indium-tin oxide, indium contact ring
- (b) Counter electrode: 2 in. glass, $\lambda/4$ polished.
- (6) Coating: 400 Å indium-tin oxide; 4 μm SiO_x liquid crystal spacers, 100 Å/5 Å shallow angle SiO_x deposition.
- (7) Cell Construction: Anodized Al-frame, 2 in. diameter window sealed.

b. Operating Conditions

Voltage Waveform: pulsed rectangular; frequency: 1 KHz.

Forward Slope Mode: depletion phase: +30 V, 980 μsec .
accumulation phase: -20 V, 20 μsec

Ring Diode Bias: +30 V, 5 mA.

c. Performance

Resolution: 50 lines/mm (4⁵ Air Force Resolution Chart)

Contrast Ratio: (at 60 $\mu\text{W}/\text{cm}^2$) - 32:1

Rise Time: 2 msec

Decay Time: 20 msec.

5. 2 Inch Silicon Liquid Crystal Light Valve No. 779

a. General

- (1) Substrate: Silicon, Wafer 7.5 ϕ ; diameter 2 in.; thickness 0.005 in.

MOS Structure: 2500 Å thermally grown oxide gate.

Back Contact: Indium-tin-oxide and aluminum.

Microchannel Grid: phosphorous ion implantation, $1 \times 10^{12}/\text{cm}^3$. 10 μm x 10 μm cell size.

Diode Guard Ring: phosphorous ion implantation $10^{13}/\text{cm}^2$.

Diameter: 1.7 in., Width: 0.015 in.

- (2) Light Blocking Layer/Dielectric Mirrors: 14 pairs Si/SiO₂.
- (3) Liquid Crystal Alignment: 45° angle-evaporated SiO_x.
- (4) Liquid Crystal: BDH E-18 biphenyl, eutectic, 4 μm thickness.
- (5) Glass Electrodes:
- (a) Substrate electrode: 2 in. fiber optic.
Coating: 500 Å indium-tin oxide, indium contact ring
- (b) Counter electrode: 2 in. glass, $\lambda/4$ polished.
- (6) Coating: 400 Å indium-tin oxide; 4 μm SiO_x liquid crystal spacers, 100 Å/5 Å shallow SiO_x deposition.
- (7) Cell Construction: Anodized Al-frame, 2 in. diameter window sealed.

b. Operating Conditions

Voltage Waveform: pulsed rectangular; frequency: 1 KHz.

Forward Slope Mode: depletion phase: +30 V, 980 μsec .
accumulation phase: -20 V, 20 μsec

Ring Diode Bias: +30 V, 2 mA.

c. Performance

Resolution: 50 lines/mm (4⁵ Air Force Resolution Chart)

Contrast Ratio: (at 60 $\mu\text{W}/\text{cm}^2$) - 23:1

Rise Time: 2 msec

Decay Time: 18 msec.

B. MULTIMODE LIQUID CRYSTAL CELLS

1. Test Cell No. 1

a. Specifications:

Twist Angle: 60°
Pre-tilt Angle: 2° to 40°
Thickness: $4.6 \mu\text{m}$
Mirror: front silver attached
Liquid Crystal: BDH E-7 biphenyl, eutectic
Glass Electrodes:

Dimensions: $1.25 \times 1.75 \times 0.5$ in., $\lambda/2$ polished
Coating: 500 \AA ITO

Cell construction: anodized aluminum frame, 2×2 in.

b. Operating Conditions

Voltage waveform: ac, 10 Hz
Voltage: 1 to 6 V rms
Input polarizer: 30°
Output analyzer: 120°

c. Performance

Colors: pink = 1.46 V, green = 1.80 V, magenta = 2.10 V,
Gray-scale white = 2.38 to 3.15 V, dark > 3.15 V
Threshold voltage: 0.95 V
Characteristic curves: See Figure 28
Switching ratio for multimode: 2.2.

d. Comments

The measured transmission characteristic curves (Figure 28) demonstrates three separated distinct colors at the low voltage regime and a TV operational back slope regime at higher voltages. The multimode operation can be accomplished with a switching ratio voltage of 2.2. The comparison with the theoretical prediction (Figure 27) is reasonable when one takes into account the tolerance of the LCLV fabrication and the slight uncertainties of the parameters of the final device.

2. Test Cell No. 2 (Delivered on 1 December 1978)

a. Specification

Twist angle: 65°
Pe-tilt angle: 2° to 4°
Thickness: 4.8 μ m
Mirror: front silver attached
Liquid crystal: BDH E-7 biphenyl, eutectic
Glass electrodes:

Dimensions: 2 in. diameter x 0.5 in., $\lambda/2$ polished
Coating: 500 Å ITO.

Cell construction: anodized aluminum frame, 4 in. diameter

b. Operating Conditions

Voltage waveform: ac, 10 kHz
Voltage: 1 to 6 V rms
Input polarizer: 32.5°
Output analyzer: 122.5°

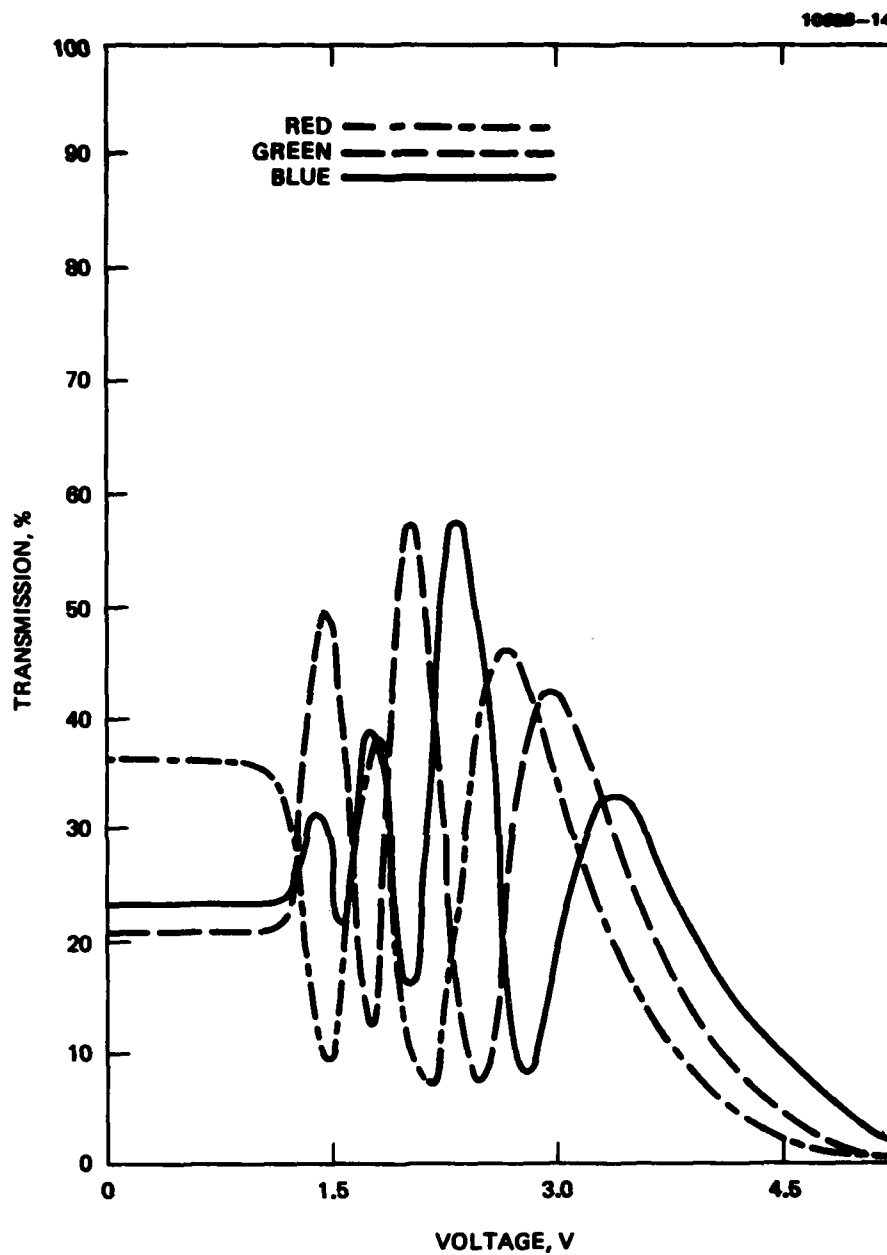


Figure 28. Measured transmission characteristic curves for multimode operation of BSM delivered liquid crystal cell. $W_m = 60^\circ$, 2° pretilt and cell thickness $L = 4.6 \mu\text{m}$.

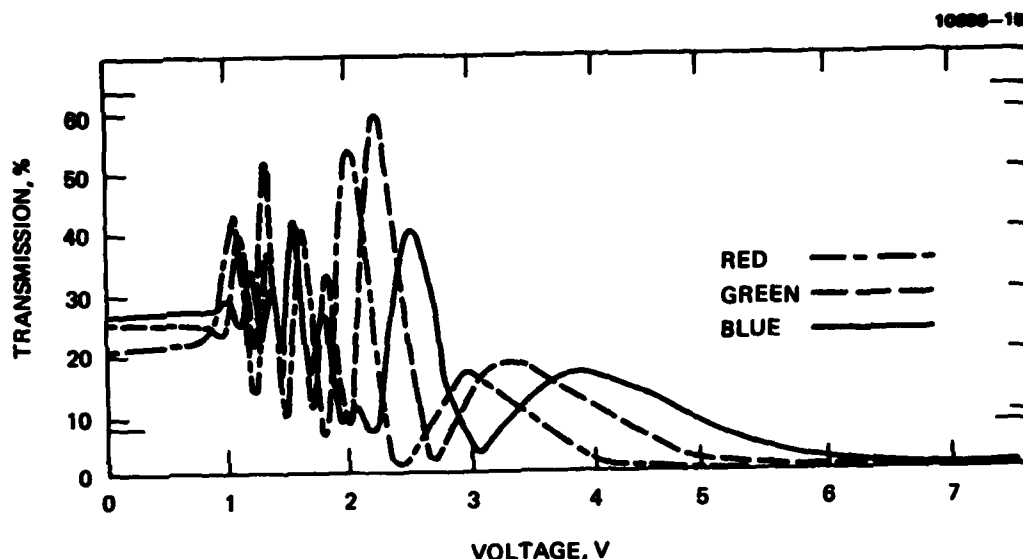


Figure 29. Measured transmission characteristic curves for BSM delivered liquid crystal cell.

c. Performance (See Figure 29)

Colors:	orange-red	2.07 V
	green	2.29 V
	blue	2.50 V
	magenta	2.71 V
	TV gray scale	3.07 to 5.54 V
	black	5.54 V

Threshold voltage: 1.23 V

d. Comments

The measured transmission characteristic curves (Figure 29) demonstrate at least four distinct colors in the low-voltage region and a TV operational back slope region at higher voltages, which can be accomplished with 2.5 switching ratio. The transmission of the TV region is rather low because of the larger variety of colors at the graphic region. The theoretical predictions are shown in Figure 30 for similar parameters and to demonstrate the effect of a tradeoff between the output transmission intensity at the high voltage region and the performance of the multicolor graphic region at low voltages. The theoretical transmission curves (Figure 30) were numerically evaluated using the following parameters:

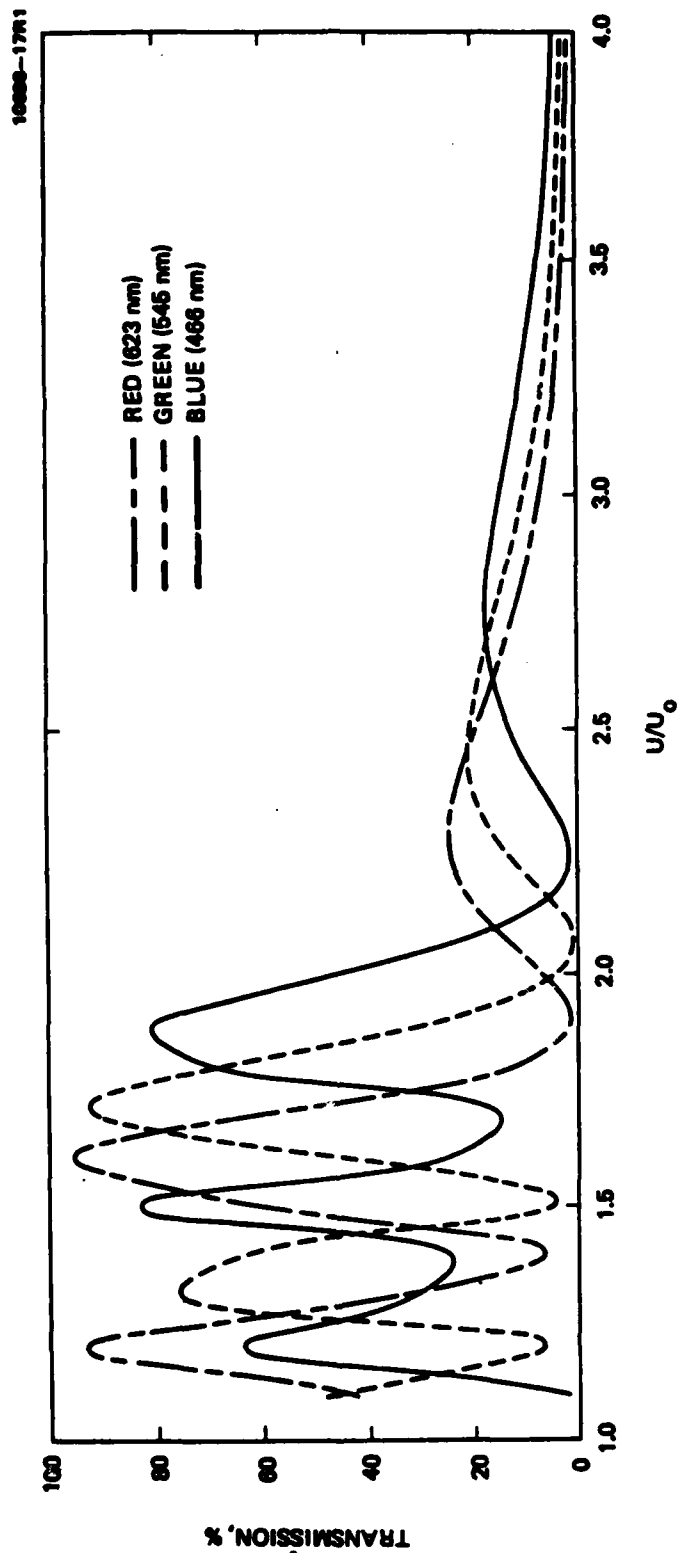


Figure 30. Theoretical transmission curves for the BSM configuration of a 5.4- μ m-thick LCLV with maximum twist, $W_m = 70^\circ$, and input polarizer angle, $i = 35^\circ$.

maximum twist angle of 70° , thickness of $5.4 \mu\text{m}$, input polarizer angle of 35° , and output analyzer at 125° . Graphs are shown for: red (623 nm), green (545 nm), and blue (466 nm) monochromatic lines. The theoretical curves predict a larger actual thickness of the LC layer in the delivered cell.

3. LCLV No. 3: 2 in. CdS Light Valve No. 10377 Test Results

a. Contrast Ratio (backslope mode) 6.8:1.

Conditions: $V_{\text{rms}} = 21.4 \text{ V}$; $f = 15 \text{ kHz}$; input light level = 75 mW/cm^2 (green); yellow background.

b. Resolution (backslope mode) 4^4 Air Force Chart = 45 lines/mm.
Conditions: same as (1) above, input light level = 20 mW/cm^2 .

c. Color Range

When biased at $18 V_{\text{rms}}$ with green input light, the following colors were obtained as a function of the input light intensity, thus demonstrating distinct colors:

$I (\text{mW/cm}^2)$	4	7	25	75
Color	Red	Yellow	Blue	Blue-Black

d. Time Response (backslope mode) $T_{\text{on}} = 10 \text{ msec}$; $T_{\text{off}} = 35 \text{ msec}$.

Conditions: $V_{\text{rms}} = 21.4 \text{ V}$; $f = 15 \text{ kHz}$.

e. Characteristic Transmission Curve (see Figure 31)

Measured by changing the biasing voltage without input light.

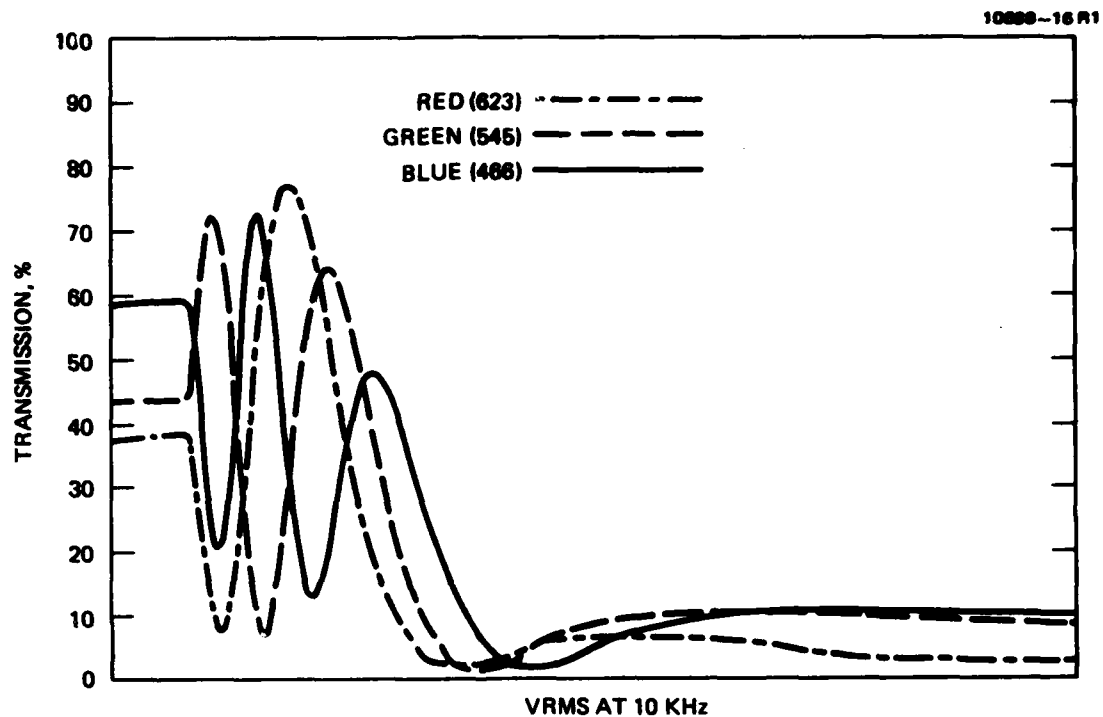


Figure 31. Measured transmission characteristic curves for delivered CdS liquid crystal light valve, demonstrating multimode operation.

SECTION 5

CONCLUSIONS AND FUTURE ISSUES

Two main issues were addressed during this program: (1) the development of a practical display device of the silicon liquid crystal light valve, and (2) the optimization of the liquid crystal parameters for multimode operation. The starting point for the first task was the already existing principle of a Si-based LCLV operating in an MOS configuration. The main issues attacked were to:

- Develop a suitable dielectric mirror/light-blocking-layer thin-film structure
- Solve the edge-breakdown problem
- Improve silicon processing in order to prevent degrading of the minority carrier lifetime and increasing the minority level of the substrate
- Scale up to a 2 in. device; wafer polish/thin down silicon processing; and light valve packaging
- Increase the resolution by improving the micro-grid and refining to 50 lines/mm.

The successful achievement of these goals resulted in the delivery of a 2 in. silicon-based LCLV featuring 50-line/mm limiting resolution, 30-msec response time (LC-limited), good contrast, and freedom from the edge-breakdown effect. The remaining issues in this program are to:

- Improve Output Uniformity

This should be based on the development of two technologies: (1) use of a non-wax wafer mounting procedure during polishing to reduce the thickness non-uniformity, and (2) use of uniform press-down of the wafer to the base electrode using optical cement. The combination of these two should result in the $\pm 10\%$ of output uniformity required.

- Microgrid Improvement

The present micro-grid with its 20- μ m cell size yields a total of 1600 TV lines at 20% MTF. This is more than sufficient for standard displays requiring 1000 TV lines or less. However, the function of this grid is to maintain the spatial pattern during the active phase by creating potential wells at the Si/SiO₂

interface. We feel that achieving the full contrast at the design resolution will require further optimization of the micro-grid. This may involve experimenting with different grid geometries and doping levels, coupled with theoretical calculations, to result in sufficiently deep potential wells. The depth of these potential wells should be such that the number of carriers, equivalent to the full input light intensity, can be maintained throughout the active phase without spill-over occurring.

In the second effort of this program, the liquid crystal studies, four tasks were addressed:

- A theoretical study of the electro-optic effects in twisted nematic liquid crystal cells.
- The numerical evaluation of characteristic curves of the LCLV under the HFE mode of operation.
- Evaluation of the effects of cell thickness, twist angle, and entrance polarization orientation.
- The Optimization of the LCLV parameters for multimode operation.

The successful achievement of these tasks resulted in computer programs for calculating the LCLV characteristic curve for any possible configuration, and for all parameters. It has also resulted in the delivery of multimode operation-optimized liquid crystal cells and light valves. The one remaining issue in this program is the application of these theoretical results to the silicon-based LCLV to fully exploit the advantages of the silicon photo substrate.

ACKNOWLEDGEMENT

The dedicated work of Miss D. Adams, Mr. A.J. Paul, Mr. P. Reif, Mr. T. Hayden and Mr. N. Goodwin, are gratefully acknowledged.

REFERENCES

1. D.W. Berreman, J. Opt. Soc. Am. 63, 1374 (1973).
2. P.O. Braatz and K. Chow, Internal Hughes Publication.
3. D.K. Schroder and H.C. Nathanson, Sol. State Elect. 13, 577 (1970).
4. C.W. Oseen, Ark. Mat. Astron. Fys. 19, 1 (1925).
5. F.C. Frank, Dis. Faraday Soc. 25, 19 (1958).
6. P.G. DeGennes, The Physics of Liquid Crystals (Clarendon Press, Oxford, 1974), pp. 59-122.
7. H.J. Deuling, Mol. Crys. Liquid, Crys. 19, 123 (1972); Ibid., 27, 81 (1974).
8. E. Wiener-Avnear and S. Singer, "A Numerical Calculation of the Electro-Optic Characteristics of the Hybrid Field Twisted Nematic Liquid Crystal Cell: Part I - The Electric Effect" (to be published).
- 9a. IMSL Library 1 Reference Manual, 6th ed., IMSLLIB-0006 (revised July 19, 1977).
- 9b. V.I. Krylov, Approximate Calculation of Integrals (MacMillan, 1962).
10. J. Grinberg and A.D. Jacobson, J. Optical Soc. A. 66, 1003 (1976).
11. E. Wiener-Avnear, "A Numerical Calculation of the Electro-Optic Characteristics of the Hybrid Field Twisted Nematic Liquid Crystal Cell: Part II - The Optic Effect" (to be published).
12. D. McIntyre and A.W. Snyder, J. Opt. Soc. A. 68, 149 (1978); D. McIntyre, Ibid. 68, 869 (1978).